SUBMISSION TO
JOURNAL OF GEOMECHANICS FOR ENERGY AND THE ENVIRONMENT
SPECIAL ISSUE ON 'LOW CARBON GEOTECHNICS'

DATE:
Written: July 2021
Revised: December 2021
Second Revision: March 2022

TITLE:
Mechanical behaviour of compacted kaolin clay stabilised via alkali activated calcium-rich fly ash binder

AUTHORS:
Elodie Coudert[a,b,c]
Giacomo Russo[d]*
Dimitri Deneele[c,e]
Alessandro Tarantino[b]

AFFILIATION:
[a]Department of Civil and Mechanical Engineering. University of Cassino and Southern Lazio, Via G. Di Biasio 43. 03043 Cassino, Italy
[b]Department of Civil and Environmental Engineering, University of Strathclyde, 75 Montrose Street, Glasgow, Scotland, G1 1XJ, United Kingdom
[c]Institut des Matériaux Jean Rouxel (IMN), Université de Nantes, CNRS, 2 rue de la Houssinière, BP 32229, 44322 Nantes Cedex 3, France
[d]Department of Earth Science, Environment and Resources, University of Napoli Federico II, Via Cinthia 21 80126, Napoli, Italy
[e]GERS-LEE, Univ Gustave Eiffel, IFSTTAR, F-44344 Bouguenais, France;

*CORRESPONDING AUTHOR:
Prof Giacomo Russo
Department of Earth Science, Environment and Resources,
University of Napoli Federico II
Via Cinthia 21 80126, Napoli, Italy
E-mail: giarusso@unina.it.

KEYWORDS
Soil stabilisation
Alkali activated material
Kaolin
Fly ash
Mechanical behaviour
Microstructure

Abstract

Locally sourced marginal earthfill geomaterials are generally not used in traditional earthfill construction due to their relatively poor mechanical performance. However, if these geomaterials are stabilised, procuring and transporting of materials from borrow sites can be avoided with significant carbon saving. Further carbon saving can be achieved by using industrial waste as binder in place of conventional high-carbon footprint stabilisers such as lime and Ordinary Portland Cement. This paper examines the use of a calcium-rich fly ash from coal combustion activated by a sodium-based alkaline solution for the treatment of non-active clay in view of its use as earthfill geomaterial. To this end, kaolinite clay/fly ash (90/10) samples were compacted, cured for different periods, saturated, and subjected to one-dimensional compression and direct shear tests. The major outcome from 1D compression tests is that stiffness is enhanced significantly even in the very short-term (1 day after alkali activation), i.e. before the binding phase starts to form. This was attributed to the changes in pore-water chemistry (increase in pH and electrolyte concentration) following the addition of the alkaline solution and the formation of aggregates in face-to-face mode. In the long term (curing time ≥28days) stiffness appeared to be further enhanced due to the formation of the binding phase. These effects were more pronounced in the low-intermediate stress range (<~700 kPa) making the alkali activation a good soil treatment for roadway embankments. Peak shear strength also appeared to be significantly enhanced in both short and long term although effects were more pronounced for curing time ≥28days following the formation of the binding phase. Ultimate shear strength is enhanced only in the long term (curing time ≥28days).

Mechanical behaviour of compacted kaolin clay stabilised via alkali activated calcium-rich fly ash binder

Coudert E, Deneele D, Russo G, Tarantino A

1 Introduction

Soft clay-rich soils are often encountered in construction sites. These soils cannot be directly used as earthfill materials and may cause problems in earthworks because of their poor mechanical performance. To improve their engineering characteristics Ordinary Portland Cement or lime are commonly used as soil stabilisers. These are associated with high carbon dioxide emissions and energy intensive processes, which increase significantly worldwide carbon footprint (Scrivener and Kirkpatrick, 2008). As a substitute, the use of Alkali Activated Materials (AAM) has received increasing attention over the last decade. In fact, AAMs present a much lower CO_2 emission process compared to traditional Ordinary Portland Cement (OPC) (Provis and van Deventer, 2014).

The CO_2 reduction associated with the replacement of OPC with AAM has been assessed for the case of concrete. Based on a lifecycle analysis, Weil et al. (2009) concluded that the Global Warming Potential (GWP) of alkali-activated fly ash concrete is approximately 70% lower than that of OPC concrete. Yang et al. (2013) demonstrated via Life Cycle Assessment including contributions due to constituent steps, production, curing, and transportation that alkali-activated concrete reduces CO_2 emissions by 25% to 57% with respect to OPC concrete at the same mechanical performance. Similar conclusions were drawn by Robayo-Salazar et al. (2018) who showed that CO_2 emissions can be reduced by 44.7% for alkali-activated binary concrete (AABC) using natural

volcanic pozzolan or granulated blast furnace slag (at equal or even higher compressive strength). In the field of soil stabilisation, Ghadir et al. (2021) developed a comparative estimation of environmental impacts of the use of OPC and alkali-activated volcanic ash in soil stabilisation using life cycle assessment LCA, limited to the production of the required cement and alkali-activated binder for stabilization of 1 m3 functional unit of clayey soil with similar shear strength. Even if the amount of AAB used was twice compared with the OPC, with reference to carbon emissions (evaluated as kgCO2-e), the AAB had a lesser impact than OPC. Zahmak et al. (2021) in a comparative LCA analysis of different AABs for soil stabilisation showed the impact of their composition on carbon footprint. They suggest to optimize the constituents of the AAB mix, possibly by reducing the alkali activators content and/or increasing the precursors content, in order to meet the required mechanical performance without compromising the environmental impact.

Recent studies have proved that alkali activated binders can be used successfully for stabilisation of a wide range of soils including clayey soil (Wilkinson et al., 2010; Singhi et al., 2016), sandy clay (Cristelo et al., 2011), marl, marlstone (Cristelo et al., 2012), silty sand (Rios et al., 2016) and road aggregates (Tenn et al., 2015). Applications have included deep soft soil improvement (Cristelo et al., 2011) and rammed earth construction (Silva et al., 2013).

However, these studies have mainly focused on soil-fly ash samples prepared form slurry state. When compacted fly ash samples were tested, investigation of mechanical properties was limited to unconfined compressive strength (UCS).

To investigate whether alkali activated fly ash can be potentially used to stabilise marginal clays in turn to be used as construction material for earth structures, compressibility and shear strength properties should be tested. From a practical point of

view, the time scale of the effects of alkali activation should also be investigated as this affects the construction process and the time required for the embankments to come into service after construction.

This paper presents an experimental investigation of the mechanical behaviour of compacted clay stabilised with alkali activated fly ash. Oedometer and direct shear tests were carried out to investigate compressibility and shear strength of the clay-fly ash mixtures, which were compacted and then cured for different periods following alkali activation. Mercury intrusion porosimetry tests were also conducted to investigate microstructural features of samples prepared by mixing clay and alkali-activated fly ash.

A calcium-rich fly ash from coal combustion was used in this study, which was activated by a sodium-based alkaline solution. Kaolin was selected as its reactivity to alkaline activation at ambient temperature is negligible, and hence it does not interfere in the reaction sequence allowing for a study of the binder effect only. Besides, kaolin represents a wide class of clays encountered in engineering projects and so it is considered here as a model soil.

2 Background

Alkali Activated Materials derive from the reaction between solid aluminosilicate powder (usually metakaolin, fly ash, blast furnace slag or natural pozzolan) and alkali metal source (most commonly alkali hydroxide and/or alkali silicate solutions) (Buchwald et al., 2003; Shi et al., 2006). The resulting material is a binder system cured at room temperature with mechanical properties and durability potentially suitable for Portland cement replacement. The supply of an alkali metal source via an alkaline solution raises the pH of the reaction mixture and accelerates the dissolution of the aluminosilicate

powder. Its dissolution releases some of its constitutive elements into the medium that combine with the ions of the alkaline solution to form a binding phase. Different binding phases are formed depending on the nature of ions dissolved from the aluminosilicate source. For example, the binding phase consists of Calcium Silicate Hydrate (as in Portland cement) if the ion released by the aluminosilicate source is calcium and consists of a three-dimensional aluminosilicate network known as a geopolymer binder if the ions released by the aluminosilicate source are mainly silicon and aluminium.

The pH generated by the supply of the alkali metal source can reach values as high as 14 according to Paudel et al. (2020), who measured pH of pore-water extracted from Alkali-Activated Fly Ash concrete. However, pH decreases over time during curing to around 13 as the hydroxyl ion OH^- is progressively consumed in the polycondensation reactions. Alkaline soils may potentially limit the availability of nutrients to plants. However, recent studies by Golek and Gula (2020) have shown that plant growth in topsoil overlying the alkali-activated binder treated soil layers is not inhibited or damaged due to the plant ability to self-regulate the pH of the environment in which they grow.

3 Materials and methods

3.1 *Materials*

A Polish fly ash derived from hard coal and coal slime combustion in fluidised bed boiler was used in this study. It consists primarily of SiO_2, Al_2O_3 and CaO (Table 1). The fly ash contains 52% of particles sized lower than 45 μm and 41% lower than 10 μm. Speswhite kaolin provided by Imerys Minerals UK was also used in this study (Table 1). It is mainly constituted of kaolinite (95%) and secondarily of muscovite (4%) (Chemeda, 2015). The kaolin contains, approximately, 100 % of particles sized lower than 10 μm

and 80 % lower than 2 μm. Its specific gravity is G_s = 2.60. The liquid and plastic limits are 70 % and 32 % respectively giving a plasticity index of 38 % (Vitale et al., 2016).

The alkaline solution used consisted of a sodium silicate aqueous solution with a molar ratio SiO_2/Na_2O of 1.7, dry mass percentage of 44%, and density of 1.55g/cm³ (supplied by Woellner Group and under the commercial name GEOSIL 34417).

3.2 Sample preparation

Sample preparation was designed to mimic the process that would be adopted in embankment construction. The alkaline solution (sodium silicate and water) was stirred for one hour (Vitale et al. 2017, Sitarz et al. 2020) and then sprayed on the mix of aluminosilicate (fly ash) and kaolin powders previously mixed together. Kaolin and fly ash were mixed in proportion 90/10 by dry mass (mix referred to as KF10) (Cristelo et al. 2012, Sargent et al. 2013, Zhang et al. 2013). This ratio is in line with the fraction of Portland cement typically added to soil to be stabilised (in the range 7 to 12 % according to Petry and Wohlgemuth, 1988).

The wet powder was statically compacted (Zhang et al. 2013, Sargent et al. 2013 Phummiphan et al. 2016, Rios et al. 2016) to a vertical stress of 600 kPa (maintained for 1h). Once the compaction load was removed, the samples were cured for 1, 7, 14, 28, 60 or 90 days at 20 °C inside their moulds. Finally, samples within their mould were stored under vacuum to avoid carbonation during curing (Coudert et al. 2019, Vitale et al. 2021).

The mould was the oedometer ring for samples to be tested in one-dimensional compression and a purposely designed 3D printed plastic mould for samples to be tested in direct shear tests.

The initial water content was fixed to 28% for all the samples, which corresponds to the optimum moisture content determined by Proctor compaction test (Sivakumar and Wheeler, 2000). Additionally, the mass ratio of alkaline solution to fly ash was fixed to 50% (Duxson et al., 2005; Criado et al., 2007, Pummihpan et al. 2019, Abdullah et al. 2019), giving the initial molar ratios (considering that kaolin is unreactive): Si/Al = 1.2, Si/Na = 2.7 and Al/Na = 2.1. It is worth noticing that the Al/Na ratio was not fixed to one, which is the value that optimises the properties of alkali activated materials. The ratio Al/Na =1 is adequate to provide a charge-balancing of the negative AlO_4^- tetrahedron charge but not in excess to promote efflorescence that may disrupt the polymerisation process (Barbosa et al., 2000). In the case examined in this work, the presence of calcium ions in high quantity plays a role of charge compensation as well as sodium and this is the reason for accepting an Al/Na ratio different from one.

3.3 Methods

3.3.1 One-dimensional compression test

Oedometer tests were performed on compacted samples in standard oedometer cell. After saturation by filling the external container with water, vertical stress σ_v was applied in steps ($\Delta\sigma_v/\sigma_v = 1$) up to 2220 kPa and then reversed. Samples were allowed to consolidate under each loading. As consolidation time t_{100} was of the order of a few minutes, total test duration could be maintained within 1 day thus avoiding significant curing inside the oedometer cell.

3.3.2 Mercury Intrusion Porosimetry (MIP)

MIP tests were carried out on samples removed from the oedometer cell at a given vertical stress in order to capture microstructural features of samples induced by loading along

the compressibility curve. MIP tests were performed on freeze dried samples by a double chamber Micromeritics Autopore III apparatus. In the filling apparatus (dilatometer) samples were outgassed under vacuum and then filled by mercury allowing increase of absolute pressure up to ambient one. Using the same unit, the intrusion pressure was than raised up to approximately 200 kPa by means of compressed air. The detected pore-entrance sizes ranged between 134 μm and 7.3 μm (approximately 0.01 MPa - 0.2 MPa for a mercury contact angle of 139°). After depressurisation to ambient pressure, samples were transferred to high-pressure unit, where mercury pressure was increased up to 205 MPa following a previously set intrusion program. The smallest detected entrance pore diameter was about 7 nm. Corrections to pore-size distribution due to compressibility of intrusion system were applied performing a blank test.

Samples tested in the MIP were obtained by imposing a vertical stress of either 714 or 1428 kPa. Two different samples for each stress level were prepared, as suggested by Pedrotti and Tarantino (2018). After reaching the target applied stress, the first sample was quickly unloaded in one single step to minimise recovering of volumetric strains (undrained conditions). The sample was then rapidly removed from the oedometer and sealed in plastic bag to prevent water loss until the freeze-drying was performed. This sample will be referred to as '*ncl*' as it was expected to maintain the microstructure of the material along the normal compression line. The second sample was unloaded under drained conditions, allowing the rebound of the structure and the recovering of elastic strains. This sample will be referred to as '*url*' as it was expected to maintain the microstructure of the material along the unloading-reloading line.

3.3.3 Direct shear test

Direct shear tests were performed according to ASTM D 3080-90 (ASTM D 3080-90, 1994) on compacted samples in a standard shear box. Cured samples were transferred to the shear box by centring the 3D printed mould onto the shear box upper half and pushing down the sample using a load frame with the help of a wooden pusher. Samples were fully saturated by filling the external container with water and vertical displacements were monitored. After saturation, a normal stress of 100 kPa or 200 kPa was applied in steps until full consolidation was achieved. The highest consolidation time t_{100} associated with primary consolidation was recorded for the kaolin alone at 100 kPa vertical stress (t_{100}=5 min). The minimum time to failure t_f in shear was then calculated according to Head (1994) as $t_f = 12.7 \cdot t_{100}$ (t_f=63.5 min). Shear displacement was applied at a rate of 0.04 mm/min, which returns a time to failure of 200 min for a total shear displacement of 8mm. The actual time to failure adopted was well in excess time the minimum time to failure calculated according to Head (1994).

3.3.4 ^{29}Si NMR spectroscopy

Solid-state ^{29}Si NMR spectroscopy was performed on i) fly ash alone and fly ash following alkali activation after 28 days and 6 months and ii) kaolinite mixed with 50% of fly ash (KF50) at 1 day, 28 days, and 6 months. These measurements were aimed at investigating the physicochemical evolution occurring in the alkali activated high-calcium fly ash.

Solid-state ^{29}Si NMR spectroscopy was performed using a Bruker Avance III 300 MHz (7 T) spectrometer and 7 mm MAS probe. ^{29}Si MAS spectra were acquired with a single $\pi/2$ pulse excitation of 5.5 μs and ^{1}H decoupling. The repetition times were 2 s, 120 s and 30 s for the raw high-calcium fly ash, the raw kaolin and all the activated samples,

210 respectively. For all ^{29}Si spectra, MAS spinning rate was set to 5 kHz. Spectra were
211 referenced against TMS (tetramethylsilane) for ^{29}Si.

212 # 4 Results

213 ## *4.1 One-dimensional compression*

214 Fig. 1 shows compressibility curves of the raw kaolin and the treated kaolin (KF10) as a
215 function of curing period. The samples with curing period of 1d and 7d show very similar
216 initial void ratio (following saturation) as the raw kaolin. Upon loading, the material
217 KF10 maintains a higher void ratio although the normal compression line attained
218 eventually appears to be parallel to the one of the raw kaolin (in a semi-log scale).
219 The sample with curing period of 14 days shows an initial void ratio (after saturation)
220 lower than raw kaolin and the KF10 samples cured for 1 and 7 days. However, its
221 compression curve re-joins the curves of samples cured for 1 and 7 days at 357 kPa.
222 The samples with curing periods of 28, 60, and 90 days also show an initial lower void
223 ratio. The compression curves are very similar and show a normal compression branch
224 higher than the one of the samples cured for 1, 7, and 14 days (although the normal
225 compression lines still appears to be parallel to the ones of samples cured for 1, 7, and 14
226 days).
227 Table 2 reports the pre-consolidation stress and the pre-yield compressibility for Pre-
228 consolidation pressure for kaolin and alkali activated binder treated kaolin (KF10) at
229 different curing periods. The treated kaolin at curing periods equal or greater than 28 days
230 shows a markedly lower compressibility than kaolin alone.
231 The unloading curves are consistent with the loading behaviour. The samples with curing
232 period of 1, 7, and 14 days, which presented similar behaviour in loading, also show

similar response in unloading and are stiffer than raw kaolin. The samples with curing period of 28, 60, and 90 days, which presented similar behaviour in loading, also show similar response in unloading and stiffer response than samples cured for 1, 7, and 14 days.

Overall, the response in compression for short curing period (1 and 7 days) appears significantly different from the one observed for long curing periods (28, 60, and 90 days). The sample cured for 14 days shows intermediate behaviour.

4.2 Pore-size distribution (PSD)

To investigate the effect of loads on the microstructure of the treated soil, mercury intrusion porosimetry analyses were performed at 28 days on treated samples subjected to either 714 or 1428 kPa. As shown in Fig. 1, the 714 kPa stress is approximately associated with the yielding stress whereas the 1428 kPa stress is associated with a post-yielding stress state. The quality of sample preparation by freeze-drying was checked by comparing the void ratio measured in a traditional way (via oven-drying) with the void ratio measured via the volume of mercury intruding the sample. As shown in Table 3, there is a fair match between the two measurements.

The pore-entrance size frequency distributions before and after unloading are shown in Fig. 2. Samples show a bimodal distribution of entrance pore diameters. As widely accepted (e.g. Delage et al., 1996; Tarantino and De Col, 2008; Russo and Modoni, 2013), microstructure of compacted treated samples is characterized by an aggregate structure, with smaller pores (associated with modal size of ~0.18 μm) corresponding to intra-aggregates pores and larger pores (associated with modal size in the range 0.6-1.0 μm) corresponding to inter-aggregates pores.

The most significant changes of microstructure induced by the applied load occurs in the inter-aggregate porosity with a shift of the larger pores (0.4 μm – 10 μm) towards smaller pore sizes (Fig. 2a). This shift remains when samples are unloaded (Fig. 2b) indicating that non-reversible deformation is associated with the change in inter-aggregate porosity, possibly associated with partial destructuration. On the other hand, the intra-aggregate pores do not appear to be affected by the applied loads.

The changes of microstructure associated with the unloading process show a similar pattern, i.e. only the inter-aggregate porosity is affected by the rebound whereas the intra-aggregate pores remain unchanged upon unloading (Fig. 2b,c).

For comparison, the pore-size distributions of samples KF10 loaded to 714 and 1428 kPa respectively is compared with the pore-size distribution of different 'untreated' kaolinite samples, two samples compacted to 1200 kPa vertical stress at water contents of 0.10 and 0.24 respectively and then saturated and one sample reconstituted from slurry and loaded to 70 kPa vertical stress (after Pedrotti, 2016). Despite the very different procedures used to prepare the kaolinite samples, the saturated kaolinite alone always exhibits a mono-modal distribution with modal size ~0.25 μm.

4.3 Shear strength

Fig. 4 shows the shearing behaviour of the raw kaolin and the fly ash-based alkali activated binder treated soil KF10 as a function of curing period for normal stresses of 100 and 200 kPa respectively. All samples show contractive behaviour upon shearing regardless of the normal stress applied and curing period.

At 100 kPa normal stress (Fig. 4a), the alkali activated treated samples KF10 at 1 and 7 days display a very similar behaviour suggesting that chemical reactions have not yet

279 taken place in such a short period. Nonetheless, the mobilised shear stress appears to be
280 higher than the raw kaolin. At 28-day curing time, the sample appears to be stiffer, shows
281 a clear peak, and an ultimate shear strength higher than the samples cured for 1 and 7
282 days.
283 At 200 kPa normal stress (Fig. 4b), the alkali activated treated samples KF10 at 7 days
284 shows a mobilised shear strength higher than the raw kaolin in the shear displacement
285 range 0-4mm and then appears to converge to the raw kaolin curve at very large shear
286 displacements. In contrast, the sample characterised by 28-day curing time exhibits a
287 mobilised shear strength always higher than the raw kaolin sample and the sample cured
288 for 7 days.
289 Normal displacements did not always level off at large shear displacements. Data were
290 therefore replotted by correcting the shear to normal stress ratio τ/σ' for dilatancy $\Delta y/\Delta x$,
291 where y and x are the normal and shear displacements respectively. Fig. 5 shows all the
292 tests at 100 kPa normal stress. Samples cured for 1 and 7 days show higher mobilised
293 shear stress in the low/medium range of shear displacements whereas the curves tend to
294 converge to the raw kaolin at high shear displacements. On the other hand, the sample
295 cured for 28 days shows significant gain with respect to the raw kaolin even at large shear
296 displacements. At large displacements, the stress ratio varies from ~0.4 for raw kaolin to
297 ~0.55 for KF10 cured for 28 days, corresponding to angles of shearing resistance equal
298 to 22° and 29° respectively.
299 Fig. 6 compares the stress-displacement curves at 100 and 200 kPa normal stress (for 7
300 and 28 days curing periods). At large displacements, the curves at 100 and 200 kPa
301 normal stress converge suggesting that the KF material does not exhibit any effective
302 cohesion c' in this range of normal stress for both curing periods. Fig. 6 also shows that

the sample cured for 28 days exhibit peak shear strength only when tested at the lower normal stress (100 kPa) and this peak essentially disappears when the normal stress is increased to 200 kPa. Finally, Fig. 6 confirms that there is substantial gain of shear strength as curing period increases from 7 to 28 days.

4.4 ^{29}Si MAS-NMR spectra

Fig. 7a shows the ^{29}Si MAS-NMR spectrum for the fly ash alone compared with the spectra of the fly ash following alkali activation (after 28 days and 6 months). The appearance of a new resonance located at -85 ppm is associated with the formation of the binding phase and it corresponds to Q^2-type silicon environments in chain structure that resembles the one of Calcium Silicate Hydrates encountered in Portland Cement (Coudert et al., 2019, Coudert et al., 2021). From 28 days to 6 months, the resonance associated with the binding phase does not change neither in amplitude nor in chemical shift value. Fig. 7b shows the ^{29}Si MAS-NMR spectra for kaolinite mixed with 50% of fly ash (KF50) at 1 day, 28 days, and 6 months (spectrum of the alkali activated fly ash alone at 28 days is also shown for reference). The formation of the new resonance located at -85 ppm associated with the binding phase is only present at 28 days and 6 months but not after 1 day. Fig. 7b also shows that the resonance associated with kaolinite at -91 ppm does not undergo any modification over time suggesting that the kaolinite has no reactivity. Although Fig. 7b shows the spectra for KF50 mixture (50% flay ash fraction), similar pattern should be expected for the KF10 mixture (10% flay ash fraction) tested in the experimental programme presented herein.

5 Discussion

This study aimed to address four research questions i) does the alkali-activated calcium-rich fly ash enhance significantly the mechanical performance of 'marginal' clay geomaterials and how the fly ash-based binder compares with other conventional binders such as Ordinary Portland Cement (OPC) and lime, ii) what is the timescale of the physicochemical processes activated by the alkaline solution and their effects on the mechanical response of the treated clay, iii) what are the mechanisms at the particle/aggregate scale controlling the macroscopic behaviour of the treated clay, and iv) what are the engineering applications where this stabilisation can be successfully envisaged.

5.1 Mechanical performance of fly-ash treated clay and comparison with cement-treated clay

As shown by the oedometer and direct shear tests results (Fig. 2 and Fig. 5 to Fig. 7), the addition of alkali activated fly ash increases significantly stiffness and shear strength at least in certain stress ranges. In Fig. 8 a comparison between the mechanical performance induced by alkali activated fly ash (KF40) and by Ordinary Portland cement (KC40) for samples prepared with the same binder content (40% by dry mass of soil) and cured for 7 and 60 days. No relevant changes in the compressibility curves are observed for KF40 and KC40 samples cured for 7 days before testing (Fig. 8A). For longer curing times, results show a higher compressibility reduction and yield stress increase for KF40 treated samples compared to cement treated samples (Fig. 8B). The post-yield behaviour induced by OPC shows the highest slope of the compressibility curve, highlighting a more evident destructuration stage for cement treated samples at increasing vertical stresses.

5.2 Timescale of binding phase formation

The binding phase does not yet form after 1 day as shown by the ^{29}Si MAS-NMR spectra for kaolinite mixed with 50% of fly ash (Fig. 7b). At the same time, the comparison between fly ash alone and fly ash following alkali activation (Fig. 7a) shows negligible evolution of the binding phase beyond 28 days. Physicochemical reactions therefore complete between 1 day and 28 days.

5.3 Micro-scale mechanisms

The one-dimensional compression tests Fig. 1 have shown three distinct behaviours. The raw kaolin shows an almost immediate transition to a normally consolidated state (compression curve liner in a semi-log plot). According to Pedrotti and Tarantino (2018), this would be associated with the progressive disengagement of edge-to-face contacts of the initially 'flocculated' fabric occurring at pH values lower the point of Zero Charge (PZC).

In contrast, the treated clay in the very short term (days 1 and 8 following the alkali activation) shows an over-consolidated behaviour and a transition to normally consolidated state in the range 357-714 kPa. Since the binding phase does not form yet after 1 day (Fig. 7b) and the compression curves after 1 and 8 days are very similar (Fig. 1), it can be inferred that the binding phase does not form even after 8 days. As a result, the different compression behaviour observed for the treated kaolinite after 1 and 8 days compared to the kaolinite alone would not be due to the formation of the binding phase but should be sought in the change of pore-water chemistry due to the addition of the alkaline solution.

The alkaline environment generated by the addition of the sodium silicate aqueous solution makes the kaolinite particles charged negatively on both edge and basal planes (Wang and Siu 2006) thus preventing the formation of aggregates by edge-to-face association (flocculated fabric). In kaolinite with negligible electrolyte concentration, this would generate a 'dispersed' fabric with significant reduction in void ratio compared with clay in acidic environment (Pedrotti and Tarantino, 2018). The increase in pH would therefore cause a reduction in void ratio rather than an increase as observed in Fig. 1.

The higher void ratio of the KF10 material cured for 1 and 8 days observed over the entire stress range can only be justified by clay particles forming stacks promoted by the reduced double-layer repulsion in turn induced by the increase of electrolyte concentration associated with the addition of the alkaline solution (electrolyte concentration would be of the order of 1 molal if Na_2O dissociated completely in water). This is in line with the observations by Vitale et al. (2016) who analysed the effect of addition of CaO that, similarly to Na_2O, also increases both pH and electrolyte concentration.

At high stress, the slope of the normal consolidation line (ncl) becomes parallel to the one of clay alone suggesting similar micro-mechanisms ruling non-reversible behaviour (Pedrotti and Tarantino, 2018). It can be speculated that stacks are orienting similarly to individual particles for the case of clay alone (Fig. 9).

In the long term (after 28, 60, and 90 days) the binding phase has formed (Fig. 7b) and this generates a further increase in the pre-consolidation stress (Fig. 1) possibly due to the bonding of the aggregates. The normal compression line (ncl) remains parallel to the one measured for samples cured for 1 and 8 days suggesting similar mechanisms for non-reversible deformation. It can therefore be speculated that the bonds are broken at high

392 stresses and the higher void ratio is simply due to the presence of an additional phase
393 filling the pore space.
394 The assumption about the aggregate fabric forming in the treated clay is corroborated by
395 pore-size distribution data. As shown in Fig. 3 , the pore-size distributions of the samples
396 KF10 loaded to 714 and 1428 kPa respectively are clearly bi-modal with modal sizes of
397 ~0.15 and ~1 μm respectively. In contrast, the saturated kaolinite alone always exhibits a
398 mono-modal distribution with modal size ~0.25 μm regardless of the sample preparation
399 procedures (by compaction or reconstitution from slurry) and hydro-mechanical history.
400 As a result, the bi-modal distribution of the treated samples as compared to the mono-
401 modal distribution of saturated kaolinite alone corroborates the assumption of aggregated
402 fabric for the treated kaolin.
403 The conceptual microstructural model laid down in Fig. 9 with reference to 1D
404 compression behaviour can also explain the effect of alkaline activation on shear strength.
405 In the short term (1 and 8 days), the aggregation induced by the change in pore-water
406 chemistry would explain the higher shear strength of the treated kaolinite compared to
407 the raw kaolinite in the intermediate horizontal displacement range (Fig. 5). At large
408 horizontal displacements, the effect of aggregation seems to be lost, which is in line with
409 the compressibility of the treated clay at 1 and 8 days recovering the same values of the
410 compressibility of the raw kaolinite at high compression stresses (Fig. 1).
411 In the long term (28 days), the binding phase generates an increase in shear strength over
412 the entire displacement range with both peak and ultimate shear strength significantly
413 enhanced by the formation of the binding phase (Fig. 6). It is worth noticing that the
414 treated clay experienced no dilatancy upon shearing (Fig. 4a). Peak shear strength is
415 therefore associated with the presence of the binding phase. The decay of shear strength

following peak in the sample tested at 100 kPa normal stress at 28 days is likely associated with partial breakage of the binding phase. This peak does not appear in the sample tested at 200 kPa normal stress at 28 days likely because the higher normal stress facilitates earlier breakage of the binding phase.

5.4 Carbon footprint evaluation

Carbon footprint of soil treated with activated fly ash was evaluated and compared with that of soil treated with Ordinary Portland cement. As mentioned in Section 5.1, KC40 and KF40 samples were prepared by adding 40% of binder (OP cement or alkali-activated fly ash repsectively) by dry weight of the clay at initial water content of 55% (equal to liquid limit of KF40). The mass fractions of each phase of samples KC40 and KF40 are reported in Table 4. The values of embodied carbon eCO_2, defined as the carbon dioxide associated with the manufacture and use of a product and expressed in kg CO_2-e/kg were derived from literature with reference to the cradle-to-gate values. The soil treated with alkaline-activated fly ash is characterised by emissions (expressed in kg CO_2-e/ton) that are 60% lower than soil treated with OP cement at very similar mechanical performance (Table 4). As widely shown in the literature, the carbon footprint of alkali-activated fly ash-treated samples is mainly associated with sodium silicate. Nonetheless, the overall emissions remain substantially lower than the soil treated with Ordinary Portland cement.

5.5 Engineering applications

Results from 1D compression tests show that there is an immediate increase in stiffness following alkaline activation in the stress range 10-700 kPa and this effect is enhanced in the long term once the binding phase forms. On the other hand, the beneficial effects in stiffness is lost at very high stress. This makes alkali activated fly ash a suitable binder

for stabilisation of marginal clays, alternative to traditional binders such as lime and/or cement. The range of stresses where this improvement technique appears to be effective well fits the typical range of stresses in embankments or earthfills, suggesting it could be applied successfully to enhance the performance of several geotechnical structures involving compaction of marginal geomaterials.

6 Conclusions

This paper has examined the use of a calcium-rich fly ash from coal combustion activated by a sodium-based alkaline solution for the treatment of non-active clay in view of its use as earthfill geomaterial.

When subjected to one-dimensional compression, the treated soil shows an increase in-pre-consolidation stress and, hence, an increase in stiffness in the stress range up to ~700 kPa. This increase is observed even in the very short-term (1 day after alkali activation), i.e. before the binding phase starts to form. This was attributed to the changes in pore-water chemistry following the addition of the alkaline solution. The increase in electrolyte concentration is assumed to deplete the double-layer repulsion and promote aggregation in face-to-face mode. The aggregated fabric of the treated kaolin was confirmed by pore-size distribution data from mercury intrusion porosimetry. In the long term (curing time ≥28days) stiffness appeared to be further enhanced due to the formation of the binding phase.

Peak shear strength also appeared to be significantly enhanced in both short and long term although effects were more pronounced for curing time ≥28days following the formation of the binding phase. Ultimate shear strength appeared to be enhanced only in the long term (curing time ≥28days) due to the presence of the binding phase creating bonding

462 between clay particles. For short curing periods, the change of pore-water chemistry does
463 not seem to affect the ultimate shear strength possibly due to the aggregates breaking
464 down. This study confirms the potential of fly ash-based alkali activated binder for
465 stabilisation of clay to be used as compacted earthfill material.
466

467 **Acknowledgements**

468 The authors wish to acknowledge the support of the European Commission via the Marie
469 Skłodowska-Curie Innovative Training Networks (ITN-ETN) project TERRE 'Training
470 Engineers and Researchers to Rethink geotechnical Engineering for a low carbon future'
471 (H2020-MSCA-ITN-2015-675762).
472

473 **References**

474 Abdullah, H.H., Shahin, M. A., Walske M. L. 2019. Geo-mechanical behavior of clay
475 soils stabilized at ambient temperature with fly-ash geopolymer-incorporated
476 granulated slag. Soils and Foundations 59 (2019) 1906–1920

477 ASTM D 3080-90, 1994. Standard test method for direct shear test of soils under
478 consolidated drained conditions. Annu. Book ASTM Stand. 04.08., 290–295.

479 Barbosa, V. F., MacKenzie, K. J.D., Thaumaturgo C. 2000. Synthesis and
480 characterisation of materials based on inorganic polymers of alumina and silica:
481 sodium polysialate polymers. International Journal of Inorganic Materials 2, no. 4
482 pp. 309–17

483 Buchwald, A., Kaps, C., Hohmann, M., 2003. Alkali-activated binders and pozzolan
484 cement binders–complete binder reaction or two sides of the same story, in:
485 Proceedings of the 11th International Conference on the Chemistry of Cement.
486 Portland Cement Association Durban, South Africa, pp. 1238–1246.

487 Chemeda, Y., 2015. Effect of hydrated lime on kaolinite surface properties and its
488 rheological behaviour. PhD Thesis, Université de Nantes, France.

489 Coudert, E., Paris, M., Deneele, D., Russo, G., Tarantino, A., 2019. Use of alkali activated
490 fly ash binder for kaolin clay soil stabilisation: Physicochemical evolution.
491 Construction and Building Materials 201 (2019) 539–552

492 Coudert, E., Deneele, D., Russo, G., Vitale, E., Tarantino, A., 2021. Microstructural
493 evolution and mechanical behaviour of alkali activated fly ash binder treated clay.
494 Construction and Building Materials 285 (2021) 122917.

495 Criado, M., Fernandez-Jimenez, A., Palomo, A. 2007. Alkali activation of fly ash: effect
496 of the Sio2/Na2O ratio – Part I: FTIR study. Microporous Mesoporous Materials;

106:180–91.

Cristelo, N., Glendinning, S., Fernandes, L., Pinto, A.T., 2012. Effect of calcium content on soil stabilisation with alkaline activation. Constr. Build. Mater. 29, 167–174. https://doi.org/10.1016/j.conbuildmat.2011.10.049

Cristelo, N., Glendinning, S., Teixeira Pinto, A., 2011. Deep soft soil improvement by alkaline activation. Proc. Inst. Civ. Eng. - Ground Improv. 164, 73–82. https://doi.org/10.1680/grim.900032

Delage, P., Audiguier, M., Cui, Y.-J., Howat, M.D., 1996. Microstructure of a compacted silt. Can. Geotech. J. 33, 150–158. https://doi.org/10.1139/t96-030

Duxson, P., Lukey, G., Separovic, F., van Deventer, J. 2005. Effect of alkali cations on aluminum incorporation in geopolymeric gels. Ind Eng Chem Res 2005;44:832–9.

Ghadir P., Zamanian M., Mahbubi-Motlagh N., Saberian M., Li J., Ranjbar N. 2021. Shear strength and life cycle assessment of volcanic ash-based geopolymer and cement stabilized soil: A comparative study. Transportation Geotechnics 31 100639. 10.1016/j.trgeo.2021.100639

Gołek, Ł., Guła, A. 2020. Effect of the alkali-activated binder on plant growth. Cement Wapno Beton, 25 (2020), 242-254. https://doi.org/10.32047/CWB.2020.25.3.7

Head, K.H., 1994. Manual of Soil Laboratory Testing Volume 2: Permeability, Shear Strength and Compressibility Tests. Second Edition, ELE International Limited.

Long G., Gao Y., Xie Y. 2015. Designing more sustainable and greener self-compacting concrete. Construction and Building Materials 84 301–306. 10.1016/j.conbuildmat.2015.02.072

Paudel, S. R., Yang, M., Gao, Z. 2020. pH Level of Pore Solution in Alkali-Activated Fly-Ash Geopolymer Concrete and Its Effect on ASR of Aggregates with Different

521 Silicate Contents. J. Mater. Civ. Eng., 2020, 32(9): 04020257
522 Pedrotti, M. 2016. An experimental investigation on the micromechanics of non-active
523 clays in saturated and partially-saturated states. PhD thesis, University of
524 Strathclyde, Glasgow, UK.
525 Pedrotti, M., Tarantino, A., 2018. An experimental investigation into the micromechanics
526 of non-active clays. Géotechnique 68(8): 666-683
527 Petry, T., and Wohlgemuth, S. K. 1988. The Effects of Pulverization on theStrength and
528 Durability of Highly Active Clay Soil Stabilized with Limeand Portland Cement. In
529 Transportation Research Record 1190, TRB, National Research Council,
530 Washington, D.C., pp. 38–45.
531 Provis, J.L., van Deventer, J.S.J. (Eds.), 2014. Alkali Activated Materials, RILEM State-
532 of-the-Art Reports. Springer Netherlands, Dordrecht.
533 Phummiphan, I., Horpibulsuk, S., Phoo-ngernkham, T., Arulrajah, A., Shen, S-L, 2016.
534 Marginal Lateritic Soil Stabilized with Calcium Carbide Residue and Fly Ash
535 Geopolymers as a Sustainable Pavement Base Material. J. Mater. Civ. Eng., 2017,
536 29(2). 10.1061/(ASCE)MT.1943-5533.0001708.
537 Rios, S., Cristelo, N., Viana da Fonseca, A., Ferreira, C., 2016. Structural Performance
538 of Alkali-Activated Soil Ash versus Soil Cement. J. Mater. Civ. Eng. 28, 4015125.
539 https://doi.org/10.1061/(ASCE)MT.1943-5533.0001398
540 Robayo-Salazar, R., Mejía-Arcila J., Mejía de Gutiérrez R., Martínez, E. 2018. Life cycle
541 assessment (LCA) of an alkali-activated binary concrete based on natural volcanic
542 pozzolan: A comparative analysis to OPC concrete. Construction and Building
543 Materials 176 (2018) 103–111. https://doi.org/10.1016/j.conbuildmat.2018.05.017
544 Russo, G., Modoni, G., 2013. Fabric changes induced by lime addition on a compacted

545 alluvial soil. Géotechnique Lett. 3, 93–97. https://doi.org/10.1680/geolett.13.026
546 Sargent, P., Hughes P. N., Rouainia M., White M. L. 2013. The use of alkali activated
547 waste binders in enhancing the mechanical properties and durability of soft alluvial
548 soils. Engineering Geology 152 (2013) 96–108. 10.1016/j.enggeo.2012.10.013
549 Scrivener, K.L., Kirkpatrick, R.J., 2008. Innovation in use and research on cementitious
550 material. Cem. Concr. Res. 38, 128–136. 10.1016/j.cemconres.2007.09.025
551 Shi, C., Krivenko, P.V., Roy, D.M., 2006. Alkali-activated cements and concretes. Taylor
552 & Francis, London ; New York.
553 Silva, R.A., Oliveira, D.V., Miranda, T., Cristelo, N., Escobar, M.C., Soares, E., 2013.
554 Rammed earth construction with granitic residual soils: The case study of northern
555 Portugal. Constr. Build. Mater. 47, 181–191.
556 https://doi.org/10.1016/j.conbuildmat.2013.05.047
557 Singhi, B., Laskar, A.I., Ahmed, M.A., 2016. Investigation on Soil–Geopolymer with
558 Slag, Fly Ash and Their Blending. Arab. J. Sci. Eng. 41, 393–400.
559 https://doi.org/10.1007/s13369-015-1677-y
560 Sitarz, M., Hager, I., Choińska, M. 2020. Evolution of Mechanical Properties with Time
561 of Fly- Ash- Based Geopolymer Mortars under the Effect of Granulated Ground
562 Blast Furnace Slag Addition. Energies 2020, 13, 1135; doi:10.3390/en13051135
563 Sivakumar, V. & Wheeler, S. J. 2000. Influence of compaction procedure on the
564 mechanical behaviour of an unsaturated compacted clay. Part 1: Wetting and
565 isotropic compression. Geotechnique 50, No. 4, 359–368.
566 Tarantino, A., De Col, E., 2008. Compaction behaviour of clay. Géotechnique 58, 199–
567 213.
568 Tenn, N., Allou, F., Petit, C., Absi, J., Rossignol, S., 2015. Formulation of new materials

569 based on geopolymer binders and different road aggregates. Ceram. Int. 41, 5812–
570 5820. https://doi.org/10.1016/j.ceramint.2015.01.010
571 Turner L. K., Collins F. G. 2013. Carbon dioxide equivalent (CO2-e) emissions: A
572 comparison between geopolymer and OPC cement concrete. Construction and
573 Building Materials 43 (2013) 125–130. 10.1016/j.conbuildmat.2013.01.023
574 Vitale, E., Deneele, D., Russo, G., Ouvrard, G., 2016. Short-term effects on physical
575 properties of lime treated kaolin. Appl. Clay Sci. 132–133, 223–231.
576 https://doi.org/10.1016/j.clay.2016.04.025
577 Vitale E., Russo G., Dell'Agli G., Ferone C., Bartolomeo C., 2017. Mechanical behaviour
578 of soil improved by alkali activated binders. Environments 2017, 4(4), 80.
579 doi.org/10.3390/environments4040080
580 Vitale, E., Deneele, D., Russo, G. 2021. Effects of carbonation on chemo-mechanical
581 behaviour of lime-treated soils. Bulletin of Engineering Geology and the
582 Environment. 80(3), pp. 2687–2700. https://doi.org/10.1007/s10064-020-02042-z
583 Wang, Y. H. & Siu, W. K. (2006). Structure characteristics and mechanical properties of
584 kaolinite soils. I. Surface charges and structural characterizations. Can. Geotech. J.
585 43, No. 6, 587–600.
586 Weil, M., Dombrowski, K., Buchwald, A., 2009. Life-cycle analysis of geopolymers. In:
587 Provis, J.L., Van Deventer, J.S.J. (Eds.), Geopolymers: Structures, Processing,
588 Properties and Industrial Applications. Woodhead Publishing Limited, Cambridge,
589 England, 10.1533/9781845696382.2.194.
590 Wilkinson, A., Haque, A., Kodikara, J., 2010. Stabilisation of clayey soils with industrial
591 by-products: part A. Proc. Inst. Civ. Eng. - Ground Improv. 163, 149–163.
592 https://doi.org/10.1680/grim.2010.163.3.149

593 Yang K.-H., Song J.-K., Song K.-I., 2013. Assessment of CO_2 reduction of alkali-
594 activated concrete. Journal of Cleaner Production 39 (2013) 265-272.
595 http://dx.doi.org/10.1016/j.jclepro.2012.08.001
596 Zahmak A., Abdallah M., Jarah B., Arab M. G. 2021. Environmental performance of
597 alkali-activated binders for ground improvement. Transportation Geotechnics 31
598 100631. 10.1016/j.trgeo.2021.100631
599 Zhang, M. Guo, H., El-Korchi, T., Zhang, G., Tao, M. 2013. Experimental feasibility
600 study of geopolymer as the next-generation soil stabilizer. Construction and Building
601 Materials 47 (2013) 1468–1478. 10.1016/j.conbuildmat.2013.06.017
602

TABLE LEGENDS

Table 1. Chemical composition (wt. %) of raw fly ash and kaolin.

Table 2. Pre-consolidation pressure for kaolin and alkali activated binder treated kaolin (KF10) at different curing periods

Table 3. Comparison of void ratio *e* determined by oven-drying and void ratio e_{MIP} measured by Mercury Intrusion Porosimetry.

Table 3. Comparison of void ratio *e* determined by oven-drying and void ratio e_{MIP} measured by Mercury Intrusion Porosimetry.

FIGURE LEGENDS

Fig. 1. One-dimensional compression tests on kaolin and alkali activated binder treated kaolin (KF10) at different curing periods.

Fig. 2. Frequency distribution of entrance pore size for alkali activated fly ash binder treated soil KF10 at 28-day curing period (ncl=samples unloaded under undrained conditions; url=samples unloaded under drained conditions). (a) Samples loaded to 714 and 1428 kPa. (b) Samples unloaded from 714 and 1428 kPa. (c) Samples loaded to and unloaded from 714 kPa. (d) Samples loaded to and unloaded from 1428 kPa.

Fig. 3. Frequency distribution of entrance pore size for alkali activated fly ash binder treated soil KF10 at 28-day curing period compared with kaolin samples i) compacted to 1200 kPa normal stress at water contents of 10% and 24% and then saturated and ii) sample reconstituted from slurry and loaded to 70 kPa normal stress (after Pedrotti 2016)

Fig. 4. Direct shear tests on kaolin and alkali activated binder treated kaolin (KF10) at different curing periods. (a) normal stress σ=100 kPa. (b) normal stress σ=200 kPa

Fig. 5. Direct shear tests on kaolin and alkali activated binder treated kaolin (KF10) at different curing periods and normal stress σ=100 kPa: shear strength data corrected for dilatancy.

641 Fig. 6. Direct shear tests on kaolin and alkali activated binder treated kaolin (KF10) at
642 curing periods 7 and 28 days and normal stresses σ=100 kPa and σ=200 kPa: shear
643 strength data corrected for dilatancy.
644
645 Fig. 7. ^{29}Si MAS-NMR spectra. (a) Raw fly ash and binder F100 at 28 days and 6 months.
646 (b) alkali activated binder F100 at 28 days and alkali activated kaolin KF50 at 1 and 28
647 days (after Coudert et al., 2019).
648
649 Fig. 8. Comparison between one dimensional compression tests on alkali activate fly
650 ash binder treated kaolin and ordinary Portland cement treated kaolin cured for 7 and 60
651 days.
652
653 Fig. 9. Conceptual model for micro-mechanical behaviour of raw kaolin and alkali
654 activated fly ash binder treated clay.
655
656
657

TABLES

Table 1. Chemical composition (wt. %) of raw fly ash and kaolin.

	SiO_2	Al_2O_3	Fe_2O_3	CaO	CaO_{free}[a]	MgO	SO_3	Na_2O	K_2O	H_2O	L.o.I.
Fly ash	39.4	19.8	7.4	18.6	5.2	1.8	4.1	2.0	1.8	0.0	1.7[b]
Kaolin	49.2	34.5	1.2	0.0	0.0	0.2	0.0	0.1	1.7	13.1	12.0[c]

[a] Free calcium oxide content
[b] L.o.I = Loss on ignition 900 °C
[c] L.o.I = Loss on ignition 1000 °C

Table 2. Pre-consolidation pressure for kaolin and alkali activated binder treated kaolin (KF10) at different curing periods

	Kaolin	KF10 1d	KF10 7d	KF10 14d	KF28 28d	KF60 60d	KF90 90d
Pre-consolidation stress [kPa]	98	610	670	750	770	790	820
Pre-yield compressibility [kPa^{-1}]	0.131	0.100	0.099	0.080	0.061	0.058	0.057

Table 3. Comparison of void ratio *e* determined by oven-drying and void ratio e_{MIP} measured by Mercury Intrusion Porosimetry.

	e	e_{MIP} – ncl	e_{MIP} – url
KF10 - 28 days - 714 kPa	1.22	1.48	1.58
KF10 - 28 days - 1428 kPa	1.10	1.41	1.39

672
673 Table 3. Comparison of void ratio *e* determined by oven-drying and void ratio e_{MIP}
674 measured by Mercury Intrusion Porosimetry.

KC40	eCO_2 ($kgCO_2$-e/kg)	Mass fraction (%)	emissions ($kgCO_2$-e/t)
clay		46.1	-
OP cement	0.82 (Turner & Collins 2013)	18.4	151.1
water	0.0003 (Long et al. 2015)	35.5	0.11
	TOTAL	100	151.2

KF40	eCO_2 ($kgCO_2$-e/kg)	Mass fraction (%)	emissions ($kgCO_2$-e/t)
clay		41.9	-
fly ash	0.027 (Turner & Collins 2013)	16.7	4.5
water[1]	0.0003 (Long et al. 2015)	37.7	0.1
sodium silicate	1.514 (Turner & Collins 2013)	3.7	55.7
	TOTAL	100	60.3

[1] pore water + water in alkaline solution

675
676
677
678

679 **FIGURES**
680

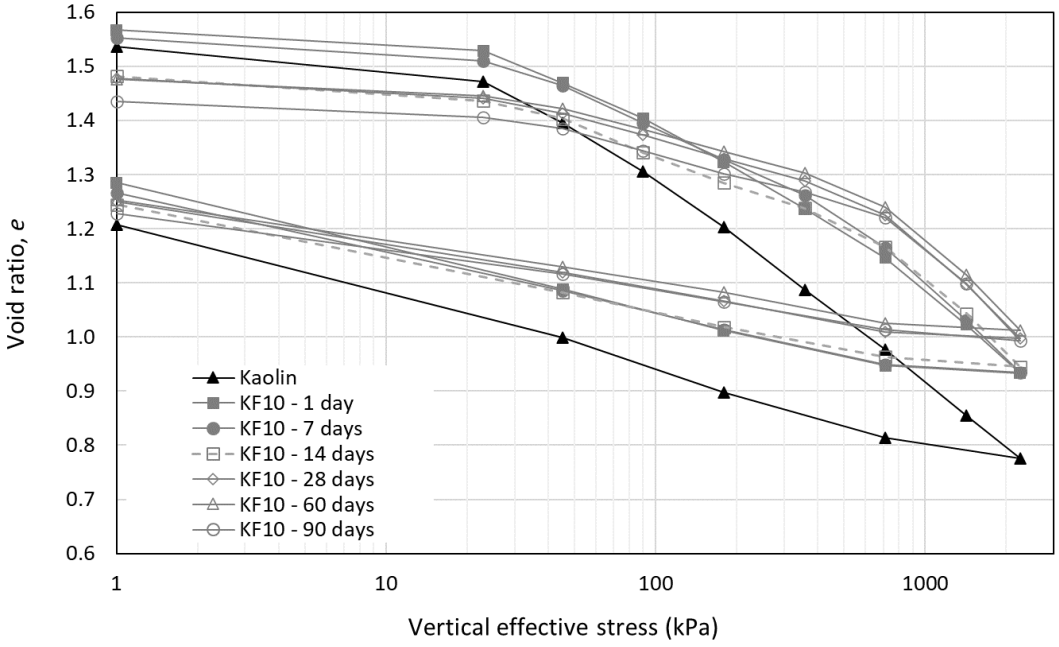

681

682 Fig. 1. One-dimensional compression tests on kaolin and alkali activated binder treated
683 kaolin (KF10) at different curing periods.

684

685

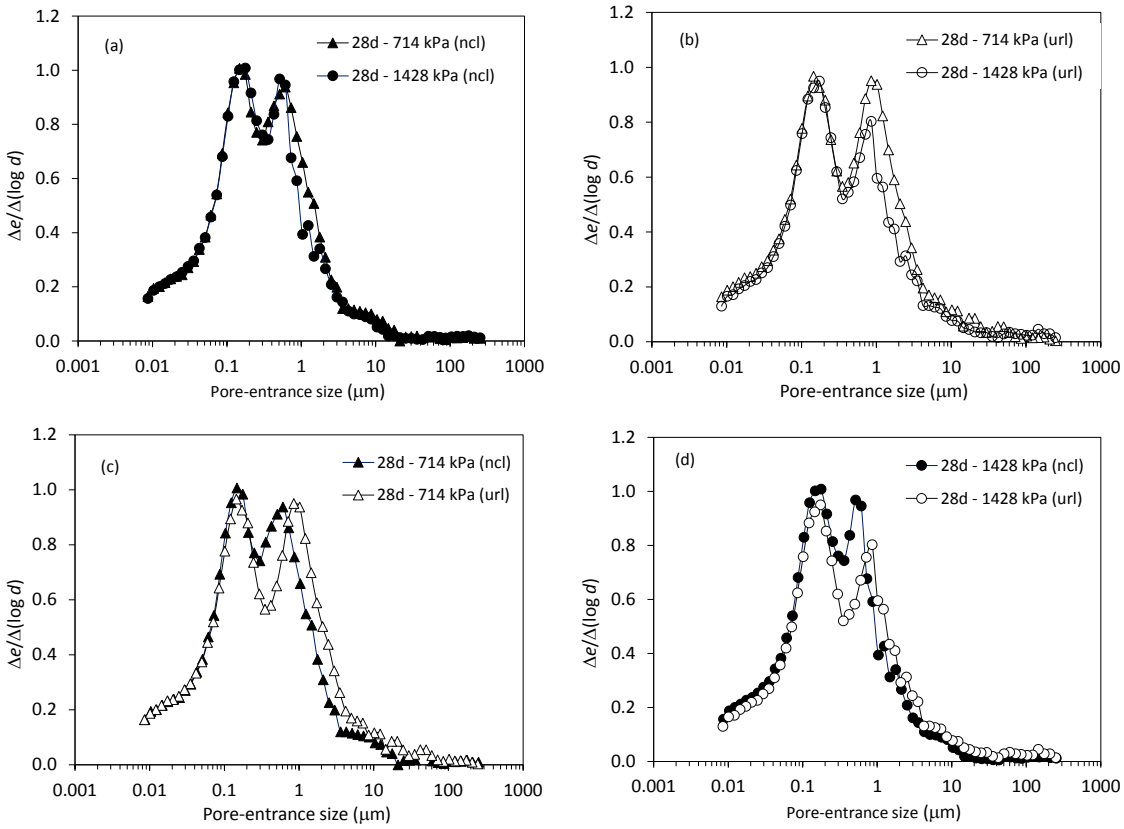

686

687 Fig. 2. Frequency distribution of entrance pore size for alkali activated fly ash binder
688 treated soil KF10 at 28-day curing period (ncl=samples unloaded under undrained
689 conditions; url=samples unloaded under drained conditions). (a) Samples loaded to 714
690 and 1428 kPa. (b) Samples unloaded from 714 and 1428 kPa. (c) Samples loaded to and
691 unloaded from 714 kPa. (d) Samples loaded to and unloaded from 1428 kPa.

692

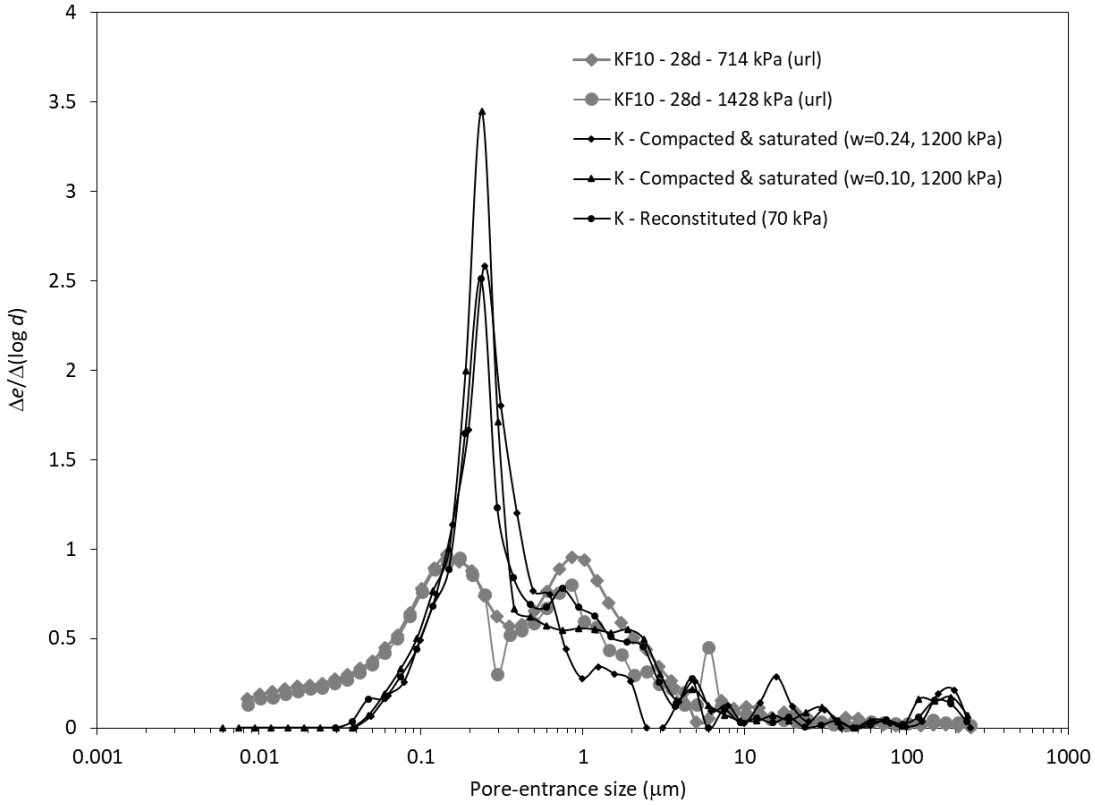

693

694 Fig. 3. Frequency distribution of entrance pore size for alkali activated fly ash binder
695 treated soil KF10 at 28-day curing period compared with kaolin samples i) compacted to
696 1200 kPa normal stress at water contents of 10% and 24% and then saturated and ii)
697 sample reconstituted from slurry and loaded to 70 kPa normal stress (after Pedrotti 2016)

698

699

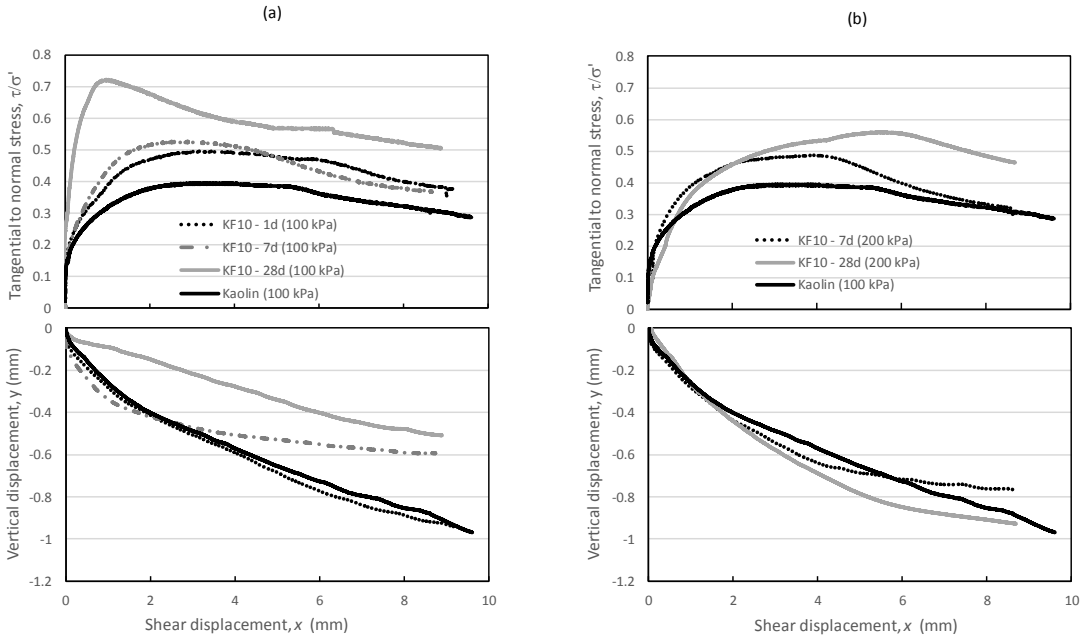

700

701

702 Fig. 4. Direct shear tests on kaolin and alkali activated binder treated kaolin (KF10) at

703 different curing periods. (a) normal stress σ=100 kPa. (b) normal stress σ=200 kPa

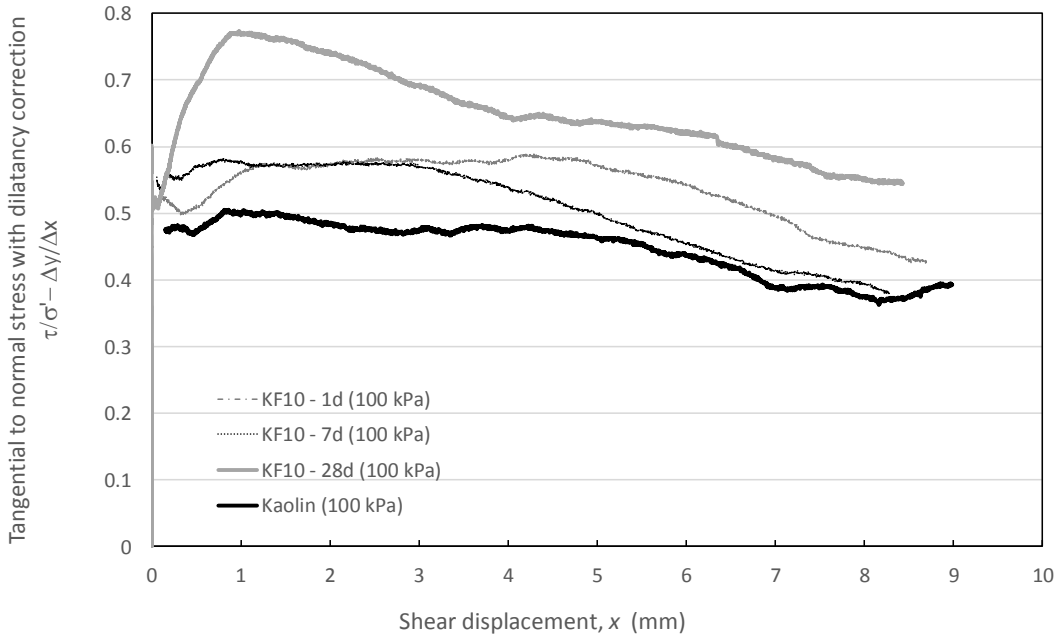

704

705 Fig. 5. Direct shear tests on kaolin and alkali activated binder treated kaolin (KF10) at
706 different curing periods and normal stress σ=100 kPa: shear strength data corrected for
707 dilatancy.

708

709

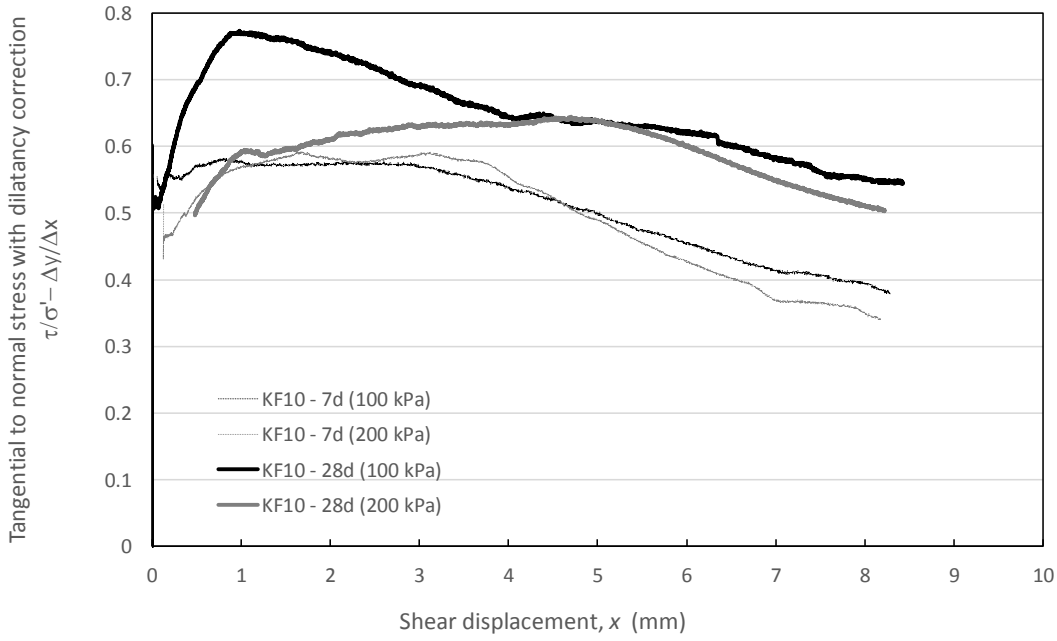

710

711 Fig. 6. Direct shear tests on kaolin and alkali activated binder treated kaolin (KF10) at
712 curing periods 7 and 28 days and normal stresses σ=100 kPa and σ=200 kPa: shear
713 strength data corrected for dilatancy.

714

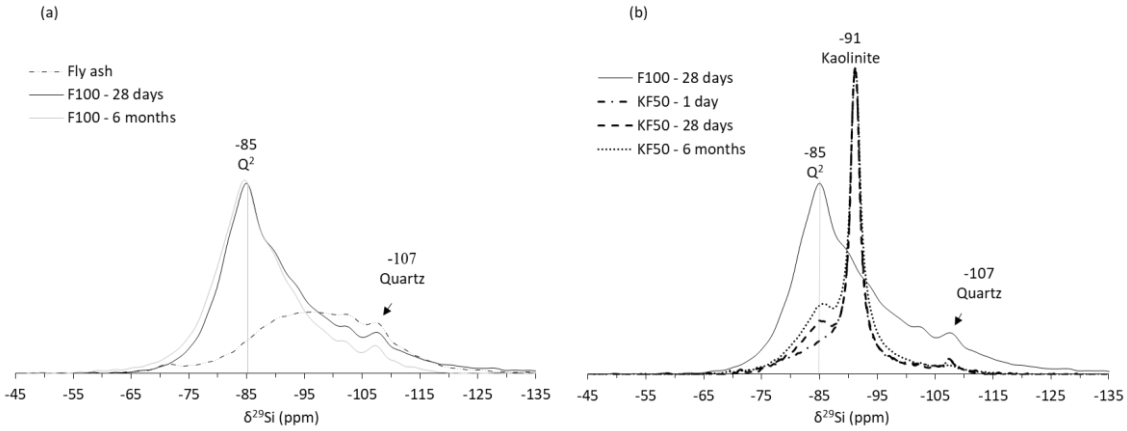

715

716

717 Fig. 7. ^{29}Si MAS-NMR spectra. (a) Raw fly ash and binder F100 at 28 days and 6

718 months. (b) alkali activated binder F100 at 28 days and alkali activated kaolin KF50 at 1

719 and 28 days (after Coudert et al., 2019).

720
721

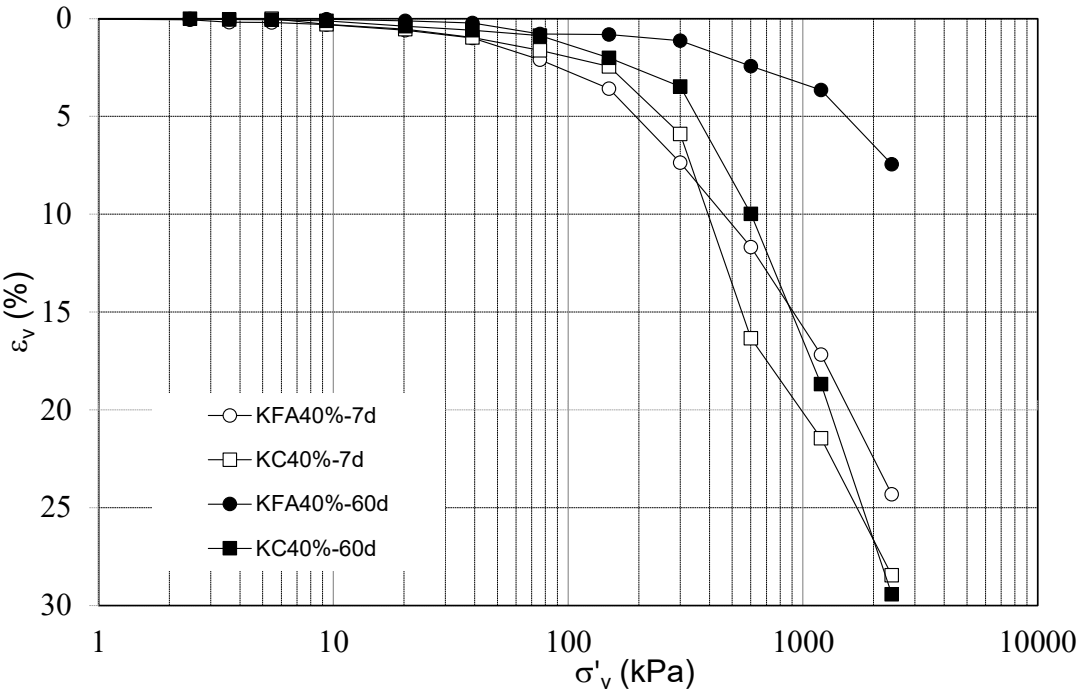

Fig. 8. Comparison between one dimensional compression tests on alkali activate fly ash binder treated kaolin and ordinary Portland cement treated kaolin cured for 7 and 60 days.

727

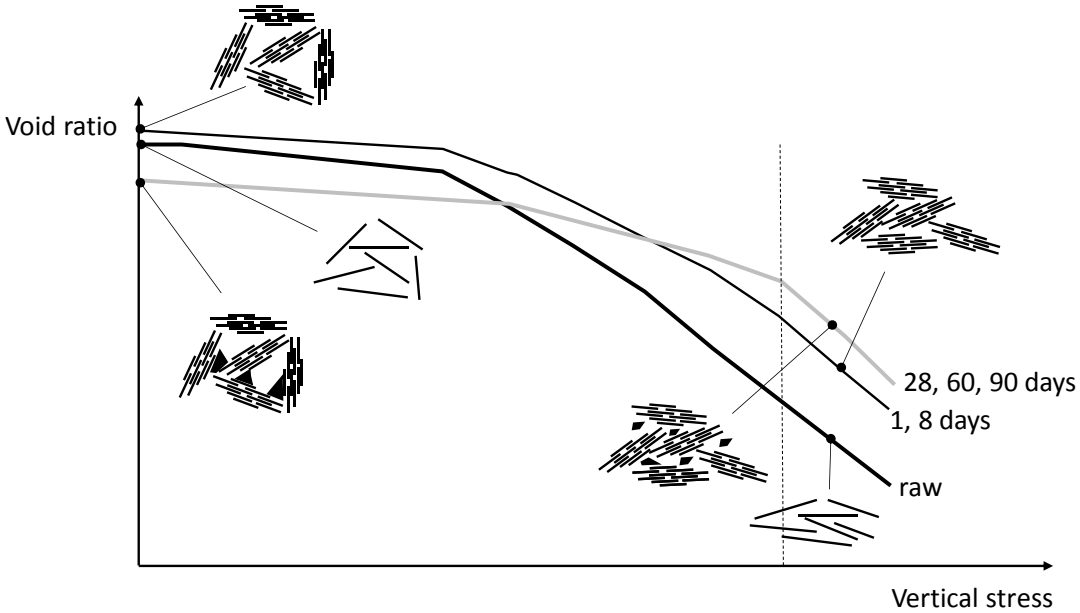

728

729 Fig. 9. Conceptual model for micro-mechanical behaviour of raw kaolin and alkali
730 activated fly ash binder treated clay.

731

732

SUBMISSION TO
JOURNAL OF GEOMECHANICS FOR ENERGY AND THE ENVIRONMENT
SPECIAL ISSUE ON 'LOW CARBON GEOTECHNICS'

DATE:
Written: July 2021
Revised: December 2021
Second Revision: March 2022

TITLE:
Mechanical behaviour of compacted kaolin clay stabilised via alkali activated calcium-rich fly ash binder

AUTHORS:
Elodie Coudert[a,b,c]
Giacomo Russo[d]*
Dimitri Deneele[c,e]
Alessandro Tarantino[b]

AFFILIATION:
[a]Department of Civil and Mechanical Engineering. University of Cassino and Southern Lazio, Via G. Di Biasio 43. 03043 Cassino, Italy
[b]Department of Civil and Environmental Engineering, University of Strathclyde, 75 Montrose Street, Glasgow, Scotland, G1 1XJ, United Kingdom
[c]Institut des Matériaux Jean Rouxel (IMN), Université de Nantes, CNRS, 2 rue de la Houssinière, BP 32229, 44322 Nantes Cedex 3, France
[d]Department of Earth Science, Environment and Resources, University of Napoli Federico II, Via Cinthia 21 80126, Napoli, Italy
[e]GERS-LEE, Univ Gustave Eiffel, IFSTTAR, F-44344 Bouguenais, France;

*CORRESPONDING AUTHOR:
Prof Giacomo Russo
Department of Earth Science, Environment and Resources,
University of Napoli Federico II
Via Cinthia 21 80126, Napoli, Italy
E-mail: giarusso@unina.it.

KEYWORDS
Soil stabilisation
Alkali activated material
Kaolin
Fly ash
Mechanical behaviour
Microstructure

Abstract

Locally sourced marginal earthfill geomaterials are generally not used in traditional earthfill construction due to their relatively poor mechanical performance. However, if these geomaterials are stabilised, procuring and transporting of materials from borrow sites can be avoided with significant carbon saving. Further carbon saving can be achieved by using industrial waste as binder in place of conventional high-carbon footprint stabilisers such as lime and Ordinary Portland Cement. This paper examines the use of a calcium-rich fly ash from coal combustion activated by a sodium-based alkaline solution for the treatment of non-active clay in view of its use as earthfill geomaterial. To this end, kaolinite clay/fly ash (90/10) samples were compacted, cured for different periods, saturated, and subjected to one-dimensional compression and direct shear tests. The major outcome from 1D compression tests is that stiffness is enhanced significantly even in the very short-term (1 day after alkali activation), i.e. before the binding phase starts to form. This was attributed to the changes in pore-water chemistry (increase in pH and electrolyte concentration) following the addition of the alkaline solution and the formation of aggregates in face-to-face mode. In the long term (curing time ≥28days) stiffness appeared to be further enhanced due to the formation of the binding phase. These effects were more pronounced in the low-intermediate stress range (<~700 kPa) making the alkali activation a good soil treatment for roadway embankments. Peak shear strength also appeared to be significantly enhanced in both short and long term although effects were more pronounced for curing time ≥28days following the formation of the binding phase. Ultimate shear strength is enhanced only in the long term (curing time ≥28days).

Mechanical behaviour of compacted kaolin clay stabilised via alkali activated calcium-rich fly ash binder

Coudert E, Deneele D, Russo G, Tarantino A

1 Introduction

Soft clay-rich soils are often encountered in construction sites. These soils cannot be directly used as earthfill materials and may cause problems in earthworks because of their poor mechanical performance. To improve their engineering characteristics Ordinary Portland Cement or lime are commonly used as soil stabilisers. These are associated with high carbon dioxide emissions and energy intensive processes, which increase significantly worldwide carbon footprint (Scrivener and Kirkpatrick, 2008). As a substitute, the use of Alkali Activated Materials (AAM) has received increasing attention over the last decade. In fact, AAMs present a much lower CO_2 emission process compared to traditional Ordinary Portland Cement (OPC) (Provis and van Deventer, 2014).

The CO_2 reduction associated with the replacement of OPC with AAM has been assessed for the case of concrete. Based on a lifecycle analysis, Weil et al. (2009) concluded that the Global Warming Potential (GWP) of alkali-activated fly ash concrete is approximately 70% lower than that of OPC concrete. Yang et al. (2013) demonstrated via Life Cycle Assessment including contributions due to constituent steps, production, curing, and transportation that alkali-activated concrete reduces CO_2 emissions by 25% to 57% with respect to OPC concrete at the same mechanical performance. Similar conclusions were drawn by Robayo-Salazar et al. (2018) who showed that CO_2 emissions can be reduced by 44.7% for alkali-activated binary concrete (AABC) using natural

volcanic pozzolan or granulated blast furnace slag (at equal or even higher compressive strength). In the field of soil stabilisation, Ghadir et al. (2021) developed a comparative estimation of environmental impacts of the use of OPC and alkali-activated volcanic ash in soil stabilisation using life cycle assessment LCA, limited to the production of the required cement and alkali-activated binder for stabilization of 1 m3 functional unit of clayey soil with similar shear strength. Even if the amount of AAB used was twice compared with the OPC, with reference to carbon emissions (evaluated as kgCO2-e), the AAB had a lesser impact than OPC. Zahmak et al. (2021) in a comparative LCA analysis of different AABs for soil stabilisation showed the impact of their composition on carbon footprint. They suggest to optimize the constituents of the AAB mix, possibly by reducing the alkali activators content and/or increasing the precursors content, in order to meet the required mechanical performance without compromising the environmental impact.

Recent studies have proved that alkali activated binders can be used successfully for stabilisation of a wide range of soils including clayey soil (Wilkinson et al., 2010; Singhi et al., 2016), sandy clay (Cristelo et al., 2011), marl, marlstone (Cristelo et al., 2012), silty sand (Rios et al., 2016) and road aggregates (Tenn et al., 2015). Applications have included deep soft soil improvement (Cristelo et al., 2011) and rammed earth construction (Silva et al., 2013).

However, these studies have mainly focused on soil-fly ash samples prepared form slurry state. When compacted fly ash samples were tested, investigation of mechanical properties was limited to unconfined compressive strength (UCS).

To investigate whether alkali activated fly ash can be potentially used to stabilise marginal clays in turn to be used as construction material for earth structures, compressibility and shear strength properties should be tested. From a practical point of

view, the time scale of the effects of alkali activation should also be investigated as this affects the construction process and the time required for the embankments to come into service after construction.

This paper presents an experimental investigation of the mechanical behaviour of compacted clay stabilised with alkali activated fly ash. Oedometer and direct shear tests were carried out to investigate compressibility and shear strength of the clay-fly ash mixtures, which were compacted and then cured for different periods following alkali activation. Mercury intrusion porosimetry tests were also conducted to investigate microstructural features of samples prepared by mixing clay and alkali-activated fly ash.

A calcium-rich fly ash from coal combustion was used in this study, which was activated by a sodium-based alkaline solution. Kaolin was selected as its reactivity to alkaline activation at ambient temperature is negligible, and hence it does not interfere in the reaction sequence allowing for a study of the binder effect only. Besides, kaolin represents a wide class of clays encountered in engineering projects and so it is considered here as a model soil.

2 Background

Alkali Activated Materials derive from the reaction between solid aluminosilicate powder (usually metakaolin, fly ash, blast furnace slag or natural pozzolan) and alkali metal source (most commonly alkali hydroxide and/or alkali silicate solutions) (Buchwald et al., 2003; Shi et al., 2006). The resulting material is a binder system cured at room temperature with mechanical properties and durability potentially suitable for Portland cement replacement. The supply of an alkali metal source via an alkaline solution raises the pH of the reaction mixture and accelerates the dissolution of the aluminosilicate

powder. Its dissolution releases some of its constitutive elements into the medium that combine with the ions of the alkaline solution to form a binding phase. Different binding phases are formed depending on the nature of ions dissolved from the aluminosilicate source. For example, the binding phase consists of Calcium Silicate Hydrate (as in Portland cement) if the ion released by the aluminosilicate source is calcium and consists of a three-dimensional aluminosilicate network known as a geopolymer binder if the ions released by the aluminosilicate source are mainly silicon and aluminium.

The pH generated by the supply of the alkali metal source can reach values as high as 14 according to Paudel et al. (2020), who measured pH of pore-water extracted from Alkali-Activated Fly Ash concrete. However, pH decreases over time during curing to around 13 as the hydroxyl ion OH^- is progressively consumed in the polycondensation reactions. Alkaline soils may potentially limit the availability of nutrients to plants. However, recent studies by Golek and Gula (2020) have shown that plant growth in topsoil overlying the alkali-activated binder treated soil layers is not inhibited or damaged due to the plant ability to self-regulate the pH of the environment in which they grow.

3 Materials and methods

3.1 *Materials*

A Polish fly ash derived from hard coal and coal slime combustion in fluidised bed boiler was used in this study. It consists primarily of SiO_2, Al_2O_3 and CaO (Table 1). The fly ash contains 52% of particles sized lower than 45 μm and 41% lower than 10 μm. Speswhite kaolin provided by Imerys Minerals UK was also used in this study (Table 1). It is mainly constituted of kaolinite (95%) and secondarily of muscovite (4%) (Chemeda, 2015). The kaolin contains, approximately, 100 % of particles sized lower than 10 μm

and 80 % lower than 2 μm. Its specific gravity is G_s = 2.60. The liquid and plastic limits are 70 % and 32 % respectively giving a plasticity index of 38 % (Vitale et al., 2016).

The alkaline solution used consisted of a sodium silicate aqueous solution with a molar ratio SiO_2/Na_2O of 1.7, dry mass percentage of 44%, and density of 1.55g/cm³ (supplied by Woellner Group and under the commercial name GEOSIL 34417).

3.2 Sample preparation

Sample preparation was designed to mimic the process that would be adopted in embankment construction. The alkaline solution (sodium silicate and water) was stirred for one hour (Vitale et al. 2017, Sitarz et al. 2020) and then sprayed on the mix of aluminosilicate (fly ash) and kaolin powders previously mixed together. Kaolin and fly ash were mixed in proportion 90/10 by dry mass (mix referred to as KF10) (Cristelo et al. 2012, Sargent et al. 2013, Zhang et al. 2013). This ratio is in line with the fraction of Portland cement typically added to soil to be stabilised (in the range 7 to 12 % according to Petry and Wohlgemuth, 1988).

The wet powder was statically compacted (Zhang et al. 2013, Sargent et al. 2013 Phummiphan et al. 2016, Rios et al. 2016) to a vertical stress of 600 kPa (maintained for 1h). Once the compaction load was removed, the samples were cured for 1, 7, 14, 28, 60 or 90 days at 20 °C inside their moulds. Finally, samples within their mould were stored under vacuum to avoid carbonation during curing (Coudert et al. 2019, Vitale et al. 2021).

The mould was the oedometer ring for samples to be tested in one-dimensional compression and a purposely designed 3D printed plastic mould for samples to be tested in direct shear tests.

The initial water content was fixed to 28% for all the samples, which corresponds to the optimum moisture content determined by Proctor compaction test (Sivakumar and Wheeler, 2000). Additionally, the mass ratio of alkaline solution to fly ash was fixed to 50% (Duxson et al., 2005; Criado et al., 2007, Pummihpan et al. 2019, Abdullah et al. 2019), giving the initial molar ratios (considering that kaolin is unreactive): Si/Al = 1.2, Si/Na = 2.7 and Al/Na = 2.1. It is worth noticing that the Al/Na ratio was not fixed to one, which is the value that optimises the properties of alkali activated materials. The ratio Al/Na =1 is adequate to provide a charge-balancing of the negative AlO_4^- tetrahedron charge but not in excess to promote efflorescence that may disrupt the polymerisation process (Barbosa et al., 2000). In the case examined in this work, the presence of calcium ions in high quantity plays a role of charge compensation as well as sodium and this is the reason for accepting an Al/Na ratio different from one.

3.3 Methods

3.3.1 One-dimensional compression test

Oedometer tests were performed on compacted samples in standard oedometer cell. After saturation by filling the external container with water, vertical stress σ_v was applied in steps ($\Delta\sigma_v/\sigma_v = 1$) up to 2220 kPa and then reversed. Samples were allowed to consolidate under each loading. As consolidation time t_{100} was of the order of a few minutes, total test duration could be maintained within 1 day thus avoiding significant curing inside the oedometer cell.

3.3.2 Mercury Intrusion Porosimetry (MIP)

MIP tests were carried out on samples removed from the oedometer cell at a given vertical stress in order to capture microstructural features of samples induced by loading along

the compressibility curve. MIP tests were performed on freeze dried samples by a double chamber Micromeritics Autopore III apparatus. In the filling apparatus (dilatometer) samples were outgassed under vacuum and then filled by mercury allowing increase of absolute pressure up to ambient one. Using the same unit, the intrusion pressure was than raised up to approximately 200 kPa by means of compressed air. The detected pore-entrance sizes ranged between 134 μm and 7.3 μm (approximately 0.01 MPa - 0.2 MPa for a mercury contact angle of 139°). After depressurisation to ambient pressure, samples were transferred to high-pressure unit, where mercury pressure was increased up to 205 MPa following a previously set intrusion program. The smallest detected entrance pore diameter was about 7 nm. Corrections to pore-size distribution due to compressibility of intrusion system were applied performing a blank test.

Samples tested in the MIP were obtained by imposing a vertical stress of either 714 or 1428 kPa. Two different samples for each stress level were prepared, as suggested by Pedrotti and Tarantino (2018). After reaching the target applied stress, the first sample was quickly unloaded in one single step to minimise recovering of volumetric strains (undrained conditions). The sample was then rapidly removed from the oedometer and sealed in plastic bag to prevent water loss until the freeze-drying was performed. This sample will be referred to as '*ncl*' as it was expected to maintain the microstructure of the material along the normal compression line. The second sample was unloaded under drained conditions, allowing the rebound of the structure and the recovering of elastic strains. This sample will be referred to as '*url*' as it was expected to maintain the microstructure of the material along the unloading-reloading line.

3.3.3 Direct shear test

Direct shear tests were performed according to ASTM D 3080-90 (ASTM D 3080-90, 1994) on compacted samples in a standard shear box. Cured samples were transferred to the shear box by centring the 3D printed mould onto the shear box upper half and pushing down the sample using a load frame with the help of a wooden pusher. Samples were fully saturated by filling the external container with water and vertical displacements were monitored. After saturation, a normal stress of 100 kPa or 200 kPa was applied in steps until full consolidation was achieved. The highest consolidation time t_{100} associated with primary consolidation was recorded for the kaolin alone at 100 kPa vertical stress (t_{100}=5 min). The minimum time to failure t_f in shear was then calculated according to Head (1994) as $t_f = 12.7 \cdot t_{100}$ (t_f=63.5 min). Shear displacement was applied at a rate of 0.04 mm/min, which returns a time to failure of 200 min for a total shear displacement of 8mm. The actual time to failure adopted was well in excess time the minimum time to failure calculated according to Head (1994).

3.3.4 ^{29}Si NMR spectroscopy

Solid-state ^{29}Si NMR spectroscopy was performed on i) fly ash alone and fly ash following alkali activation after 28 days and 6 months and ii) kaolinite mixed with 50% of fly ash (KF50) at 1 day, 28 days, and 6 months. These measurements were aimed at investigating the physicochemical evolution occurring in the alkali activated high-calcium fly ash.

Solid-state ^{29}Si NMR spectroscopy was performed using a Bruker Avance III 300 MHz (7 T) spectrometer and 7 mm MAS probe. ^{29}Si MAS spectra were acquired with a single $\pi/2$ pulse excitation of 5.5 μs and ^{1}H decoupling. The repetition times were 2 s, 120 s and 30 s for the raw high-calcium fly ash, the raw kaolin and all the activated samples,

respectively. For all ^{29}Si spectra, MAS spinning rate was set to 5 kHz. Spectra were referenced against TMS (tetramethylsilane) for ^{29}Si.

4 Results

4.1 One-dimensional compression

Fig. 1 shows compressibility curves of the raw kaolin and the treated kaolin (KF10) as a function of curing period. The samples with curing period of 1d and 7d show very similar initial void ratio (following saturation) as the raw kaolin. Upon loading, the material KF10 maintains a higher void ratio although the normal compression line attained eventually appears to be parallel to the one of the raw kaolin (in a semi-log scale).

The sample with curing period of 14 days shows an initial void ratio (after saturation) lower than raw kaolin and the KF10 samples cured for 1 and 7 days. However, its compression curve re-joins the curves of samples cured for 1 and 7 days at 357 kPa.

The samples with curing periods of 28, 60, and 90 days also show an initial lower void ratio. The compression curves are very similar and show a normal compression branch higher than the one of the samples cured for 1, 7, and 14 days (although the normal compression lines still appears to be parallel to the ones of samples cured for 1, 7, and 14 days).

Table 2 reports the pre-consolidation stress and the pre-yield compressibility for Pre-consolidation pressure for kaolin and alkali activated binder treated kaolin (KF10) at different curing periods. The treated kaolin at curing periods equal or greater than 28 days shows a markedly lower compressibility than kaolin alone.

The unloading curves are consistent with the loading behaviour. The samples with curing period of 1, 7, and 14 days, which presented similar behaviour in loading, also show

similar response in unloading and are stiffer than raw kaolin. The samples with curing period of 28, 60, and 90 days, which presented similar behaviour in loading, also show similar response in unloading and stiffer response than samples cured for 1, 7, and 14 days.

Overall, the response in compression for short curing period (1 and 7 days) appears significantly different from the one observed for long curing periods (28, 60, and 90 days). The sample cured for 14 days shows intermediate behaviour.

4.2 Pore-size distribution (PSD)

To investigate the effect of loads on the microstructure of the treated soil, mercury intrusion porosimetry analyses were performed at 28 days on treated samples subjected to either 714 or 1428 kPa. As shown in Fig. 1, the 714 kPa stress is approximately associated with the yielding stress whereas the 1428 kPa stress is associated with a post-yielding stress state. The quality of sample preparation by freeze-drying was checked by comparing the void ratio measured in a traditional way (via oven-drying) with the void ratio measured via the volume of mercury intruding the sample. As shown in Table 3, there is a fair match between the two measurements.

The pore-entrance size frequency distributions before and after unloading are shown in Fig. 2. Samples show a bimodal distribution of entrance pore diameters. As widely accepted (e.g. Delage et al., 1996; Tarantino and De Col, 2008; Russo and Modoni, 2013), microstructure of compacted treated samples is characterized by an aggregate structure, with smaller pores (associated with modal size of ~0.18 μm) corresponding to intra-aggregates pores and larger pores (associated with modal size in the range 0.6-1.0 μm) corresponding to inter-aggregates pores.

The most significant changes of microstructure induced by the applied load occurs in the inter-aggregate porosity with a shift of the larger pores (0.4 μm – 10 μm) towards smaller pore sizes (Fig. 2a). This shift remains when samples are unloaded (Fig. 2b) indicating that non-reversible deformation is associated with the change in inter-aggregate porosity, possibly associated with partial destructuration. On the other hand, the intra-aggregate pores do not appear to be affected by the applied loads.

The changes of microstructure associated with the unloading process show a similar pattern, i.e. only the inter-aggregate porosity is affected by the rebound whereas the intra-aggregate pores remain unchanged upon unloading (Fig. 2b,c).

For comparison, the pore-size distributions of samples KF10 loaded to 714 and 1428 kPa respectively is compared with the pore-size distribution of different 'untreated' kaolinite samples, two samples compacted to 1200 kPa vertical stress at water contents of 0.10 and 0.24 respectively and then saturated and one sample reconstituted from slurry and loaded to 70 kPa vertical stress (after Pedrotti, 2016). Despite the very different procedures used to prepare the kaolinite samples, the saturated kaolinite alone always exhibits a mono-modal distribution with modal size ~0.25 μm.

4.3 Shear strength

Fig. 4 shows the shearing behaviour of the raw kaolin and the fly ash-based alkali activated binder treated soil KF10 as a function of curing period for normal stresses of 100 and 200 kPa respectively. All samples show contractive behaviour upon shearing regardless of the normal stress applied and curing period.

At 100 kPa normal stress (Fig. 4a), the alkali activated treated samples KF10 at 1 and 7 days display a very similar behaviour suggesting that chemical reactions have not yet

taken place in such a short period. Nonetheless, the mobilised shear stress appears to be higher than the raw kaolin. At 28-day curing time, the sample appears to be stiffer, shows a clear peak, and an ultimate shear strength higher than the samples cured for 1 and 7 days.

At 200 kPa normal stress (Fig. 4b), the alkali activated treated samples KF10 at 7 days shows a mobilised shear strength higher than the raw kaolin in the shear displacement range 0-4mm and then appears to converge to the raw kaolin curve at very large shear displacements. In contrast, the sample characterised by 28-day curing time exhibits a mobilised shear strength always higher than the raw kaolin sample and the sample cured for 7 days.

Normal displacements did not always level off at large shear displacements. Data were therefore replotted by correcting the shear to normal stress ratio τ/σ' for dilatancy $\Delta y/\Delta x$, where y and x are the normal and shear displacements respectively. Fig. 5 shows all the tests at 100 kPa normal stress. Samples cured for 1 and 7 days show higher mobilised shear stress in the low/medium range of shear displacements whereas the curves tend to converge to the raw kaolin at high shear displacements. On the other hand, the sample cured for 28 days shows significant gain with respect to the raw kaolin even at large shear displacements. At large displacements, the stress ratio varies from ~0.4 for raw kaolin to ~0.55 for KF10 cured for 28 days, corresponding to angles of shearing resistance equal to 22° and 29° respectively.

Fig. 6 compares the stress-displacement curves at 100 and 200 kPa normal stress (for 7 and 28 days curing periods). At large displacements, the curves at 100 and 200 kPa normal stress converge suggesting that the KF material does not exhibit any effective cohesion c' in this range of normal stress for both curing periods. Fig. 6 also shows that

the sample cured for 28 days exhibit peak shear strength only when tested at the lower normal stress (100 kPa) and this peak essentially disappears when the normal stress is increased to 200 kPa. Finally, Fig. 6 confirms that there is substantial gain of shear strength as curing period increases from 7 to 28 days.

4.4 ^{29}Si MAS-NMR spectra

Fig. 7a shows the ^{29}Si MAS-NMR spectrum for the fly ash alone compared with the spectra of the fly ash following alkali activation (after 28 days and 6 months). The appearance of a new resonance located at -85 ppm is associated with the formation of the binding phase and it corresponds to Q^2-type silicon environments in chain structure that resembles the one of Calcium Silicate Hydrates encountered in Portland Cement (Coudert et al., 2019, Coudert et al., 2021). From 28 days to 6 months, the resonance associated with the binding phase does not change neither in amplitude nor in chemical shift value. Fig. 7b shows the ^{29}Si MAS-NMR spectra for kaolinite mixed with 50% of fly ash (KF50) at 1 day, 28 days, and 6 months (spectrum of the alkali activated fly ash alone at 28 days is also shown for reference). The formation of the new resonance located at -85 ppm associated with the binding phase is only present at 28 days and 6 months but not after 1 day. Fig. 7b also shows that the resonance associated with kaolinite at -91 ppm does not undergo any modification over time suggesting that the kaolinite has no reactivity. Although Fig. 7b shows the spectra for KF50 mixture (50% flay ash fraction), similar pattern should be expected for the KF10 mixture (10% flay ash fraction) tested in the experimental programme presented herein.

5 Discussion

This study aimed to address four research questions i) does the alkali-activated calcium-rich fly ash enhance significantly the mechanical performance of 'marginal' clay geomaterials and how the fly ash-based binder compares with other conventional binders such as Ordinary Portland Cement (OPC) and lime, ii) what is the timescale of the physicochemical processes activated by the alkaline solution and their effects on the mechanical response of the treated clay, iii) what are the mechanisms at the particle/aggregate scale controlling the macroscopic behaviour of the treated clay, and iv) what are the engineering applications where this stabilisation can be successfully envisaged.

5.1 Mechanical performance of fly-ash treated clay and comparison with cement-treated clay

As shown by the oedometer and direct shear tests results (Fig. 2 and Fig. 5 to Fig. 7), the addition of alkali activated fly ash increases significantly stiffness and shear strength at least in certain stress ranges. In Fig. 8 a comparison between the mechanical performance induced by alkali activated fly ash (KF40) and by Ordinary Portland cement (KC40) for samples prepared with the same binder content (40% by dry mass of soil) and cured for 7 and 60 days. No relevant changes in the compressibility curves are observed for KF40 and KC40 samples cured for 7 days before testing (Fig. 8A). For longer curing times, results show a higher compressibility reduction and yield stress increase for KF40 treated samples compared to cement treated samples (Fig. 8B). The post-yield behaviour induced by OPC shows the highest slope of the compressibility curve, highlighting a more evident destructuration stage for cement treated samples at increasing vertical stresses.

5.2 Timescale of binding phase formation

The binding phase does not yet form after 1 day as shown by the ^{29}Si MAS-NMR spectra for kaolinite mixed with 50% of fly ash (Fig. 7b). At the same time, the comparison between fly ash alone and fly ash following alkali activation (Fig. 7a) shows negligible evolution of the binding phase beyond 28 days. Physicochemical reactions therefore complete between 1 day and 28 days.

5.3 Micro-scale mechanisms

The one-dimensional compression tests Fig. 1 have shown three distinct behaviours. The raw kaolin shows an almost immediate transition to a normally consolidated state (compression curve liner in a semi-log plot). According to Pedrotti and Tarantino (2018), this would be associated with the progressive disengagement of edge-to-face contacts of the initially 'flocculated' fabric occurring at pH values lower the point of Zero Charge (PZC).

In contrast, the treated clay in the very short term (days 1 and 8 following the alkali activation) shows an over-consolidated behaviour and a transition to normally consolidated state in the range 357-714 kPa. Since the binding phase does not form yet after 1 day (Fig. 7b) and the compression curves after 1 and 8 days are very similar (Fig. 1), it can be inferred that the binding phase does not form even after 8 days. As a result, the different compression behaviour observed for the treated kaolinite after 1 and 8 days compared to the kaolinite alone would not be due to the formation of the binding phase but should be sought in the change of pore-water chemistry due to the addition of the alkaline solution.

The alkaline environment generated by the addition of the sodium silicate aqueous solution makes the kaolinite particles charged negatively on both edge and basal planes (Wang and Siu 2006) thus preventing the formation of aggregates by edge-to-face association (flocculated fabric). In kaolinite with negligible electrolyte concentration, this would generate a 'dispersed' fabric with significant reduction in void ratio compared with clay in acidic environment (Pedrotti and Tarantino, 2018). The increase in pH would therefore cause a reduction in void ratio rather than an increase as observed in Fig. 1.

The higher void ratio of the KF10 material cured for 1 and 8 days observed over the entire stress range can only be justified by clay particles forming stacks promoted by the reduced double-layer repulsion in turn induced by the increase of electrolyte concentration associated with the addition of the alkaline solution (electrolyte concentration would be of the order of 1 molal if Na_2O dissociated completely in water). This is in line with the observations by Vitale et al. (2016) who analysed the effect of addition of CaO that, similarly to Na_2O, also increases both pH and electrolyte concentration.

At high stress, the slope of the normal consolidation line (ncl) becomes parallel to the one of clay alone suggesting similar micro-mechanisms ruling non-reversible behaviour (Pedrotti and Tarantino, 2018). It can be speculated that stacks are orienting similarly to individual particles for the case of clay alone (Fig. 9).

In the long term (after 28, 60, and 90 days) the binding phase has formed (Fig. 7b) and this generates a further increase in the pre-consolidation stress (Fig. 1) possibly due to the bonding of the aggregates. The normal compression line (ncl) remains parallel to the one measured for samples cured for 1 and 8 days suggesting similar mechanisms for non-reversible deformation. It can therefore be speculated that the bonds are broken at high

392 stresses and the higher void ratio is simply due to the presence of an additional phase
393 filling the pore space.
394 The assumption about the aggregate fabric forming in the treated clay is corroborated by
395 pore-size distribution data. As shown in Fig. 3 , the pore-size distributions of the samples
396 KF10 loaded to 714 and 1428 kPa respectively are clearly bi-modal with modal sizes of
397 ~0.15 and ~1 μm respectively. In contrast, the saturated kaolinite alone always exhibits a
398 mono-modal distribution with modal size ~0.25 μm regardless of the sample preparation
399 procedures (by compaction or reconstitution from slurry) and hydro-mechanical history.
400 As a result, the bi-modal distribution of the treated samples as compared to the mono-
401 modal distribution of saturated kaolinite alone corroborates the assumption of aggregated
402 fabric for the treated kaolin.
403 The conceptual microstructural model laid down in Fig. 9 with reference to 1D
404 compression behaviour can also explain the effect of alkaline activation on shear strength.
405 In the short term (1 and 8 days), the aggregation induced by the change in pore-water
406 chemistry would explain the higher shear strength of the treated kaolinite compared to
407 the raw kaolinite in the intermediate horizontal displacement range (Fig. 5). At large
408 horizontal displacements, the effect of aggregation seems to be lost, which is in line with
409 the compressibility of the treated clay at 1 and 8 days recovering the same values of the
410 compressibility of the raw kaolinite at high compression stresses (Fig. 1).
411 In the long term (28 days), the binding phase generates an increase in shear strength over
412 the entire displacement range with both peak and ultimate shear strength significantly
413 enhanced by the formation of the binding phase (Fig. 6). It is worth noticing that the
414 treated clay experienced no dilatancy upon shearing (Fig. 4a). Peak shear strength is
415 therefore associated with the presence of the binding phase. The decay of shear strength

following peak in the sample tested at 100 kPa normal stress at 28 days is likely associated with partial breakage of the binding phase. This peak does not appear in the sample tested at 200 kPa normal stress at 28 days likely because the higher normal stress facilitates earlier breakage of the binding phase.

5.4 Carbon footprint evaluation

Carbon footprint of soil treated with activated fly ash was evaluated and compared with that of soil treated with Ordinary Portland cement. As mentioned in Section 5.1, KC40 and KF40 samples were prepared by adding 40% of binder (OP cement or alkali-activated fly ash repsectively) by dry weight of the clay at initial water content of 55% (equal to liquid limit of KF40). The mass fractions of each phase of samples KC40 and KF40 are reported in Table 4. The values of embodied carbon eCO_2, defined as the carbon dioxide associated with the manufacture and use of a product and expressed in kg CO_2-e/kg were derived from literature with reference to the cradle-to-gate values. The soil treated with alkaline-activated fly ash is characterised by emissions (expressed in kg CO_2-e/ton) that are 60% lower than soil treated with OP cement at very similar mechanical performance (Table 4). As widely shown in the literature, the carbon footprint of alkali-activated fly ash-treated samples is mainly associated with sodium silicate. Nonetheless, the overall emissions remain substantially lower than the soil treated with Ordinary Portland cement.

5.5 Engineering applications

Results from 1D compression tests show that there is an immediate increase in stiffness following alkaline activation in the stress range 10-700 kPa and this effect is enhanced in the long term once the binding phase forms. On the other hand, the beneficial effects in stiffness is lost at very high stress. This makes alkali activated fly ash a suitable binder

for stabilisation of marginal clays, alternative to traditional binders such as lime and/or cement. The range of stresses where this improvement technique appears to be effective well fits the typical range of stresses in embankments or earthfills, suggesting it could be applied successfully to enhance the performance of several geotechnical structures involving compaction of marginal geomaterials.

6 Conclusions

This paper has examined the use of a calcium-rich fly ash from coal combustion activated by a sodium-based alkaline solution for the treatment of non-active clay in view of its use as earthfill geomaterial.

When subjected to one-dimensional compression, the treated soil shows an increase in-pre-consolidation stress and, hence, an increase in stiffness in the stress range up to ~700 kPa. This increase is observed even in the very short-term (1 day after alkali activation), i.e. before the binding phase starts to form. This was attributed to the changes in pore-water chemistry following the addition of the alkaline solution. The increase in electrolyte concentration is assumed to deplete the double-layer repulsion and promote aggregation in face-to-face mode. The aggregated fabric of the treated kaolin was confirmed by pore-size distribution data from mercury intrusion porosimetry. In the long term (curing time ≥28days) stiffness appeared to be further enhanced due to the formation of the binding phase.

Peak shear strength also appeared to be significantly enhanced in both short and long term although effects were more pronounced for curing time ≥28days following the formation of the binding phase. Ultimate shear strength appeared to be enhanced only in the long term (curing time ≥28days) due to the presence of the binding phase creating bonding

462 between clay particles. For short curing periods, the change of pore-water chemistry does
463 not seem to affect the ultimate shear strength possibly due to the aggregates breaking
464 down. This study confirms the potential of fly ash-based alkali activated binder for
465 stabilisation of clay to be used as compacted earthfill material.
466

467 **Acknowledgements**

468 The authors wish to acknowledge the support of the European Commission via the Marie
469 Skłodowska-Curie Innovative Training Networks (ITN-ETN) project TERRE 'Training
470 Engineers and Researchers to Rethink geotechnical Engineering for a low carbon future'
471 (H2020-MSCA-ITN-2015-675762).
472

473 **References**

474 Abdullah, H.H., Shahin, M. A., Walske M. L. 2019. Geo-mechanical behavior of clay
475 soils stabilized at ambient temperature with fly-ash geopolymer-incorporated
476 granulated slag. Soils and Foundations 59 (2019) 1906–1920

477 ASTM D 3080-90, 1994. Standard test method for direct shear test of soils under
478 consolidated drained conditions. Annu. Book ASTM Stand. 04.08., 290–295.

479 Barbosa, V. F., MacKenzie, K. J.D., Thaumaturgo C. 2000. Synthesis and
480 characterisation of materials based on inorganic polymers of alumina and silica:
481 sodium polysialate polymers. International Journal of Inorganic Materials 2, no. 4
482 pp. 309–17

483 Buchwald, A., Kaps, C., Hohmann, M., 2003. Alkali-activated binders and pozzolan
484 cement binders–complete binder reaction or two sides of the same story, in:
485 Proceedings of the 11th International Conference on the Chemistry of Cement.
486 Portland Cement Association Durban, South Africa, pp. 1238–1246.

487 Chemeda, Y., 2015. Effect of hydrated lime on kaolinite surface properties and its
488 rheological behaviour. PhD Thesis, Université de Nantes, France.

489 Coudert, E., Paris, M., Deneele, D., Russo, G., Tarantino, A., 2019. Use of alkali activated
490 fly ash binder for kaolin clay soil stabilisation: Physicochemical evolution.
491 Construction and Building Materials 201 (2019) 539–552

492 Coudert, E., Deneele, D., Russo, G., Vitale, E., Tarantino, A., 2021. Microstructural
493 evolution and mechanical behaviour of alkali activated fly ash binder treated clay.
494 Construction and Building Materials 285 (2021) 122917.

495 Criado, M., Fernandez-Jimenez, A., Palomo, A. 2007. Alkali activation of fly ash: effect
496 of the Sio2/Na2O ratio – Part I: FTIR study. Microporous Mesoporous Materials;

106:180–91.

Cristelo, N., Glendinning, S., Fernandes, L., Pinto, A.T., 2012. Effect of calcium content on soil stabilisation with alkaline activation. Constr. Build. Mater. 29, 167–174. https://doi.org/10.1016/j.conbuildmat.2011.10.049

Cristelo, N., Glendinning, S., Teixeira Pinto, A., 2011. Deep soft soil improvement by alkaline activation. Proc. Inst. Civ. Eng. - Ground Improv. 164, 73–82. https://doi.org/10.1680/grim.900032

Delage, P., Audiguier, M., Cui, Y.-J., Howat, M.D., 1996. Microstructure of a compacted silt. Can. Geotech. J. 33, 150–158. https://doi.org/10.1139/t96-030

Duxson, P., Lukey, G., Separovic, F., van Deventer, J. 2005. Effect of alkali cations on aluminum incorporation in geopolymeric gels. Ind Eng Chem Res 2005;44:832–9.

Ghadir P., Zamanian M., Mahbubi-Motlagh N., Saberian M., Li J., Ranjbar N. 2021. Shear strength and life cycle assessment of volcanic ash-based geopolymer and cement stabilized soil: A comparative study. Transportation Geotechnics 31 100639. 10.1016/j.trgeo.2021.100639

Gołek, Ł., Guła, A. 2020. Effect of the alkali-activated binder on plant growth. Cement Wapno Beton, 25 (2020), 242-254. https://doi.org/10.32047/CWB.2020.25.3.7

Head, K.H., 1994. Manual of Soil Laboratory Testing Volume 2: Permeability, Shear Strength and Compressibility Tests. Second Edition, ELE International Limited.

Long G., Gao Y., Xie Y. 2015. Designing more sustainable and greener self-compacting concrete. Construction and Building Materials 84 301–306. 10.1016/j.conbuildmat.2015.02.072

Paudel, S. R., Yang, M., Gao, Z. 2020. pH Level of Pore Solution in Alkali-Activated Fly-Ash Geopolymer Concrete and Its Effect on ASR of Aggregates with Different

521 Silicate Contents. J. Mater. Civ. Eng., 2020, 32(9): 04020257
522 Pedrotti, M. 2016. An experimental investigation on the micromechanics of non-active
523 clays in saturated and partially-saturated states. PhD thesis, University of
524 Strathclyde, Glasgow, UK.
525 Pedrotti, M., Tarantino, A., 2018. An experimental investigation into the micromechanics
526 of non-active clays. Géotechnique 68(8): 666-683
527 Petry, T., and Wohlgemuth, S. K. 1988. The Effects of Pulverization on theStrength and
528 Durability of Highly Active Clay Soil Stabilized with Limeand Portland Cement. In
529 Transportation Research Record 1190, TRB, National Research Council,
530 Washington, D.C., pp. 38–45.
531 Provis, J.L., van Deventer, J.S.J. (Eds.), 2014. Alkali Activated Materials, RILEM State-
532 of-the-Art Reports. Springer Netherlands, Dordrecht.
533 Phummiphan, I., Horpibulsuk, S., Phoo-ngernkham, T., Arulrajah, A., Shen, S-L, 2016.
534 Marginal Lateritic Soil Stabilized with Calcium Carbide Residue and Fly Ash
535 Geopolymers as a Sustainable Pavement Base Material. J. Mater. Civ. Eng., 2017,
536 29(2). 10.1061/(ASCE)MT.1943-5533.0001708.
537 Rios, S., Cristelo, N., Viana da Fonseca, A., Ferreira, C., 2016. Structural Performance
538 of Alkali-Activated Soil Ash versus Soil Cement. J. Mater. Civ. Eng. 28, 4015125.
539 https://doi.org/10.1061/(ASCE)MT.1943-5533.0001398
540 Robayo-Salazar, R., Mejía-Arcila J., Mejía de Gutiérrez R., Martínez, E. 2018. Life cycle
541 assessment (LCA) of an alkali-activated binary concrete based on natural volcanic
542 pozzolan: A comparative analysis to OPC concrete. Construction and Building
543 Materials 176 (2018) 103–111. https://doi.org/10.1016/j.conbuildmat.2018.05.017
544 Russo, G., Modoni, G., 2013. Fabric changes induced by lime addition on a compacted

545 alluvial soil. Géotechnique Lett. 3, 93–97. https://doi.org/10.1680/geolett.13.026
546 Sargent, P., Hughes P. N., Rouainia M., White M. L. 2013. The use of alkali activated
547 waste binders in enhancing the mechanical properties and durability of soft alluvial
548 soils. Engineering Geology 152 (2013) 96–108. 10.1016/j.enggeo.2012.10.013
549 Scrivener, K.L., Kirkpatrick, R.J., 2008. Innovation in use and research on cementitious
550 material. Cem. Concr. Res. 38, 128–136. 10.1016/j.cemconres.2007.09.025
551 Shi, C., Krivenko, P.V., Roy, D.M., 2006. Alkali-activated cements and concretes. Taylor
552 & Francis, London ; New York.
553 Silva, R.A., Oliveira, D.V., Miranda, T., Cristelo, N., Escobar, M.C., Soares, E., 2013.
554 Rammed earth construction with granitic residual soils: The case study of northern
555 Portugal. Constr. Build. Mater. 47, 181–191.
556 https://doi.org/10.1016/j.conbuildmat.2013.05.047
557 Singhi, B., Laskar, A.I., Ahmed, M.A., 2016. Investigation on Soil–Geopolymer with
558 Slag, Fly Ash and Their Blending. Arab. J. Sci. Eng. 41, 393–400.
559 https://doi.org/10.1007/s13369-015-1677-y
560 Sitarz, M., Hager, I., Choińska, M. 2020. Evolution of Mechanical Properties with Time
561 of Fly- Ash- Based Geopolymer Mortars under the Effect of Granulated Ground
562 Blast Furnace Slag Addition. Energies 2020, 13, 1135; doi:10.3390/en13051135
563 Sivakumar, V. & Wheeler, S. J. 2000. Influence of compaction procedure on the
564 mechanical behaviour of an unsaturated compacted clay. Part 1: Wetting and
565 isotropic compression. Geotechnique 50, No. 4, 359–368.
566 Tarantino, A., De Col, E., 2008. Compaction behaviour of clay. Géotechnique 58, 199–
567 213.
568 Tenn, N., Allou, F., Petit, C., Absi, J., Rossignol, S., 2015. Formulation of new materials

based on geopolymer binders and different road aggregates. Ceram. Int. 41, 5812–5820. https://doi.org/10.1016/j.ceramint.2015.01.010

Turner L. K., Collins F. G. 2013. Carbon dioxide equivalent (CO2-e) emissions: A comparison between geopolymer and OPC cement concrete. Construction and Building Materials 43 (2013) 125–130. 10.1016/j.conbuildmat.2013.01.023

Vitale, E., Deneele, D., Russo, G., Ouvrard, G., 2016. Short-term effects on physical properties of lime treated kaolin. Appl. Clay Sci. 132–133, 223–231. https://doi.org/10.1016/j.clay.2016.04.025

Vitale E., Russo G., Dell'Agli G., Ferone C., Bartolomeo C., 2017. Mechanical behaviour of soil improved by alkali activated binders. Environments 2017, 4(4), 80. doi.org/10.3390/environments4040080

Vitale, E., Deneele, D., Russo, G. 2021. Effects of carbonation on chemo-mechanical behaviour of lime-treated soils. Bulletin of Engineering Geology and the Environment. 80(3), pp. 2687–2700. https://doi.org/10.1007/s10064-020-02042-z

Wang, Y. H. & Siu, W. K. (2006). Structure characteristics and mechanical properties of kaolinite soils. I. Surface charges and structural characterizations. Can. Geotech. J. 43, No. 6, 587–600.

Weil, M., Dombrowski, K., Buchwald, A., 2009. Life-cycle analysis of geopolymers. In: Provis, J.L., Van Deventer, J.S.J. (Eds.), Geopolymers: Structures, Processing, Properties and Industrial Applications. Woodhead Publishing Limited, Cambridge, England, 10.1533/9781845696382.2.194.

Wilkinson, A., Haque, A., Kodikara, J., 2010. Stabilisation of clayey soils with industrial by-products: part A. Proc. Inst. Civ. Eng. - Ground Improv. 163, 149–163. https://doi.org/10.1680/grim.2010.163.3.149

593 Yang K.-H., Song J.-K., Song K.-I., 2013. Assessment of CO_2 reduction of alkali-
594 activated concrete. Journal of Cleaner Production 39 (2013) 265-272.
595 http://dx.doi.org/10.1016/j.jclepro.2012.08.001
596 Zahmak A., Abdallah M., Jarah B., Arab M. G. 2021. Environmental performance of
597 alkali-activated binders for ground improvement. Transportation Geotechnics 31
598 100631. 10.1016/j.trgeo.2021.100631
599 Zhang, M. Guo, H., El-Korchi, T., Zhang, G., Tao, M. 2013. Experimental feasibility
600 study of geopolymer as the next-generation soil stabilizer. Construction and Building
601 Materials 47 (2013) 1468–1478. 10.1016/j.conbuildmat.2013.06.017
602

TABLE LEGENDS

Table 1. Chemical composition (wt. %) of raw fly ash and kaolin.

Table 2. Pre-consolidation pressure for kaolin and alkali activated binder treated kaolin (KF10) at different curing periods

Table 3. Comparison of void ratio *e* determined by oven-drying and void ratio e_{MIP} measured by Mercury Intrusion Porosimetry.

Table 3. Comparison of void ratio *e* determined by oven-drying and void ratio e_{MIP} measured by Mercury Intrusion Porosimetry.

FIGURE LEGENDS

Fig. 1. One-dimensional compression tests on kaolin and alkali activated binder treated kaolin (KF10) at different curing periods.

Fig. 2. Frequency distribution of entrance pore size for alkali activated fly ash binder treated soil KF10 at 28-day curing period (ncl=samples unloaded under undrained conditions; url=samples unloaded under drained conditions). (a) Samples loaded to 714 and 1428 kPa. (b) Samples unloaded from 714 and 1428 kPa. (c) Samples loaded to and unloaded from 714 kPa. (d) Samples loaded to and unloaded from 1428 kPa.

Fig. 3. Frequency distribution of entrance pore size for alkali activated fly ash binder treated soil KF10 at 28-day curing period compared with kaolin samples i) compacted to 1200 kPa normal stress at water contents of 10% and 24% and then saturated and ii) sample reconstituted from slurry and loaded to 70 kPa normal stress (after Pedrotti 2016)

Fig. 4. Direct shear tests on kaolin and alkali activated binder treated kaolin (KF10) at different curing periods. (a) normal stress σ=100 kPa. (b) normal stress σ=200 kPa

Fig. 5. Direct shear tests on kaolin and alkali activated binder treated kaolin (KF10) at different curing periods and normal stress σ=100 kPa: shear strength data corrected for dilatancy.

641 Fig. 6. Direct shear tests on kaolin and alkali activated binder treated kaolin (KF10) at
642 curing periods 7 and 28 days and normal stresses σ=100 kPa and σ=200 kPa: shear
643 strength data corrected for dilatancy.
644
645 Fig. 7. ^{29}Si MAS-NMR spectra. (a) Raw fly ash and binder F100 at 28 days and 6 months.
646 (b) alkali activated binder F100 at 28 days and alkali activated kaolin KF50 at 1 and 28
647 days (after Coudert et al., 2019).
648
649 Fig. 8. Comparison between one dimensional compression tests on alkali activate fly
650 ash binder treated kaolin and ordinary Portland cement treated kaolin cured for 7 and 60
651 days.
652
653 Fig. 9. Conceptual model for micro-mechanical behaviour of raw kaolin and alkali
654 activated fly ash binder treated clay.
655
656
657

TABLES

Table 1. Chemical composition (wt. %) of raw fly ash and kaolin.

	SiO_2	Al_2O_3	Fe_2O_3	CaO	CaO_{free}[a]	MgO	SO_3	Na_2O	K_2O	H_2O	L.o.I.
Fly ash	39.4	19.8	7.4	18.6	5.2	1.8	4.1	2.0	1.8	0.0	1.7[b]
Kaolin	49.2	34.5	1.2	0.0	0.0	0.2	0.0	0.1	1.7	13.1	12.0[c]

[a] Free calcium oxide content
[b] L.o.I = Loss on ignition 900 °C
[c] L.o.I = Loss on ignition 1000 °C

Table 2. Pre-consolidation pressure for kaolin and alkali activated binder treated kaolin (KF10) at different curing periods

	Kaolin	KF10 1d	KF10 7d	KF10 14d	KF28 28d	KF60 60d	KF90 90d
Pre-consolidation stress [kPa]	98	610	670	750	770	790	820
Pre-yield compressibility [kPa^{-1}]	0.131	0.100	0.099	0.080	0.061	0.058	0.057

Table 3. Comparison of void ratio *e* determined by oven-drying and void ratio e_{MIP} measured by Mercury Intrusion Porosimetry.

	e	e_{MIP} – ncl	e_{MIP} – url
KF10 - 28 days - 714 kPa	1.22	1.48	1.58
KF10 - 28 days - 1428 kPa	1.10	1.41	1.39

672
673 Table 3. Comparison of void ratio *e* determined by oven-drying and void ratio e_{MIP}
674 measured by Mercury Intrusion Porosimetry.

KC40	eCO_2 ($kgCO_2$-e/kg)	Mass fraction (%)	emissions ($kgCO_2$-e/t)
clay		46.1	-
OP cement	0.82 (Turner & Collins 2013)	18.4	151.1
water	0.0003 (Long et al. 2015)	35.5	0.11
	TOTAL	100	151.2

KF40	eCO_2 ($kgCO_2$-e/kg)	Mass fraction (%)	emissions ($kgCO_2$-e/t)
clay		41.9	-
fly ash	0.027 (Turner & Collins 2013)	16.7	4.5
water[1]	0.0003 (Long et al. 2015)	37.7	0.1
sodium silicate	1.514 (Turner & Collins 2013)	3.7	55.7
	TOTAL	100	60.3

[1] pore water + water in alkaline solution

675
676
677
678

679 **FIGURES**
680

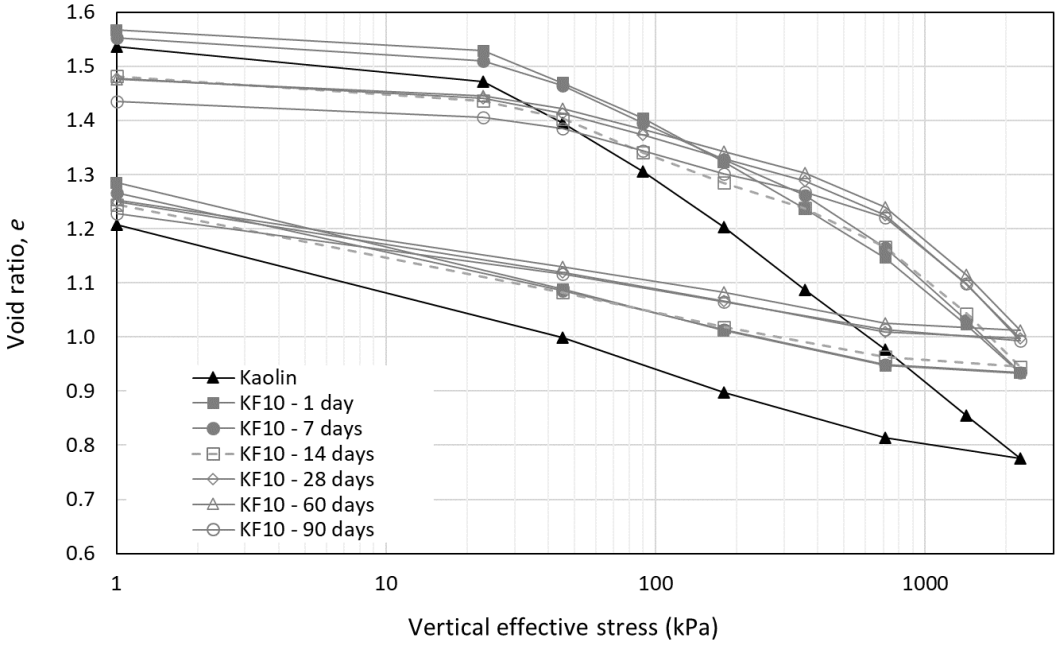

681

682 Fig. 1. One-dimensional compression tests on kaolin and alkali activated binder treated
683 kaolin (KF10) at different curing periods.

684

685

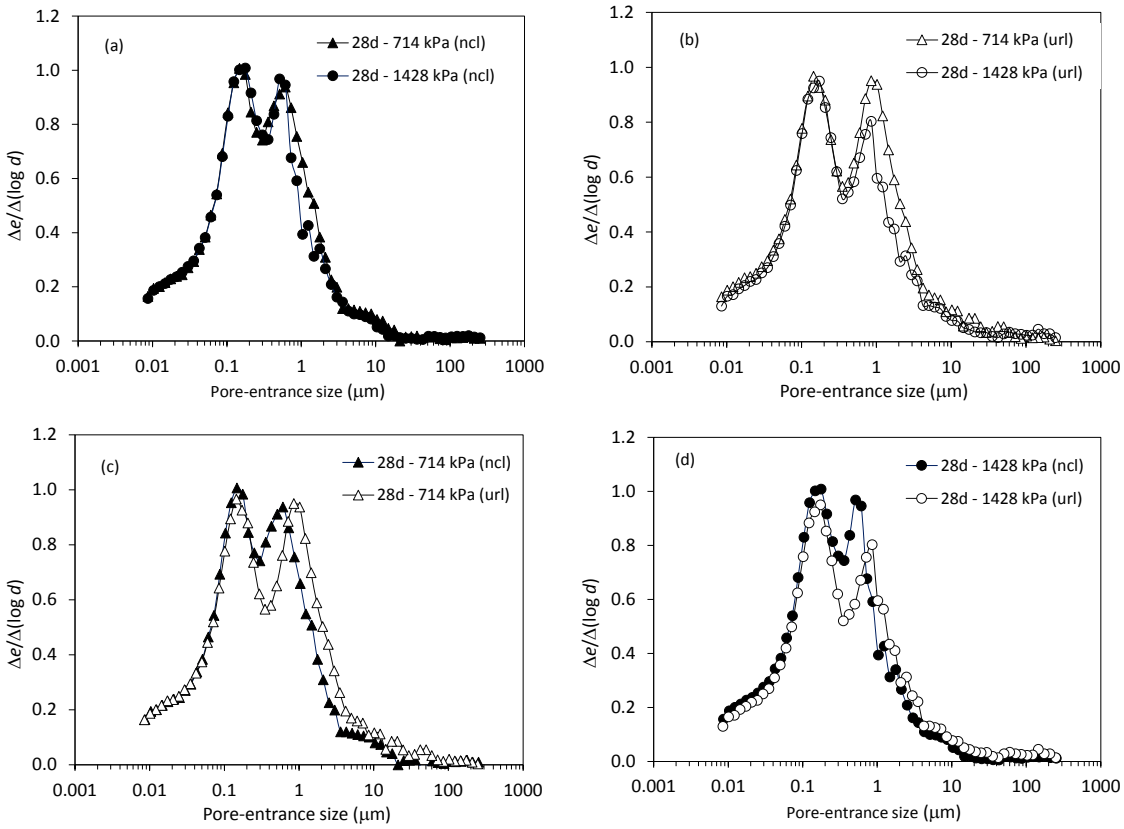

686

687 Fig. 2. Frequency distribution of entrance pore size for alkali activated fly ash binder
688 treated soil KF10 at 28-day curing period (ncl=samples unloaded under undrained
689 conditions; url=samples unloaded under drained conditions). (a) Samples loaded to 714
690 and 1428 kPa. (b) Samples unloaded from 714 and 1428 kPa. (c) Samples loaded to and
691 unloaded from 714 kPa. (d) Samples loaded to and unloaded from 1428 kPa.

692

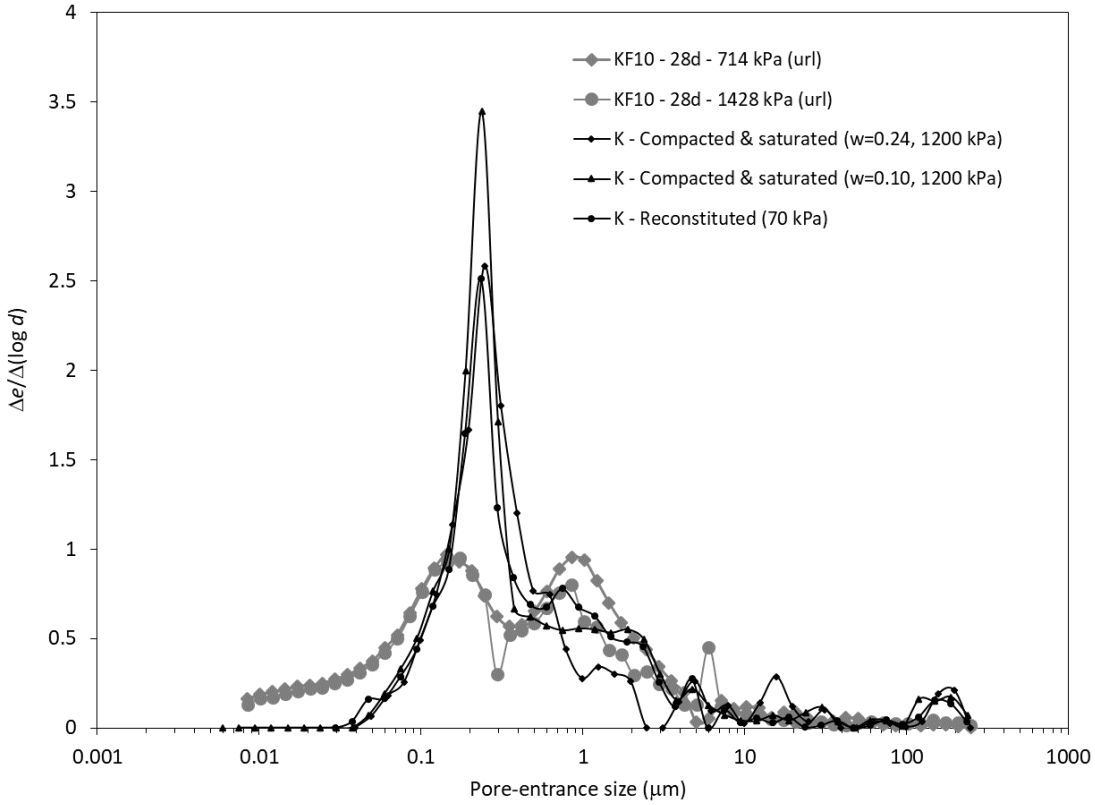

693

694 Fig. 3. Frequency distribution of entrance pore size for alkali activated fly ash binder
695 treated soil KF10 at 28-day curing period compared with kaolin samples i) compacted to
696 1200 kPa normal stress at water contents of 10% and 24% and then saturated and ii)
697 sample reconstituted from slurry and loaded to 70 kPa normal stress (after Pedrotti 2016)

698

699

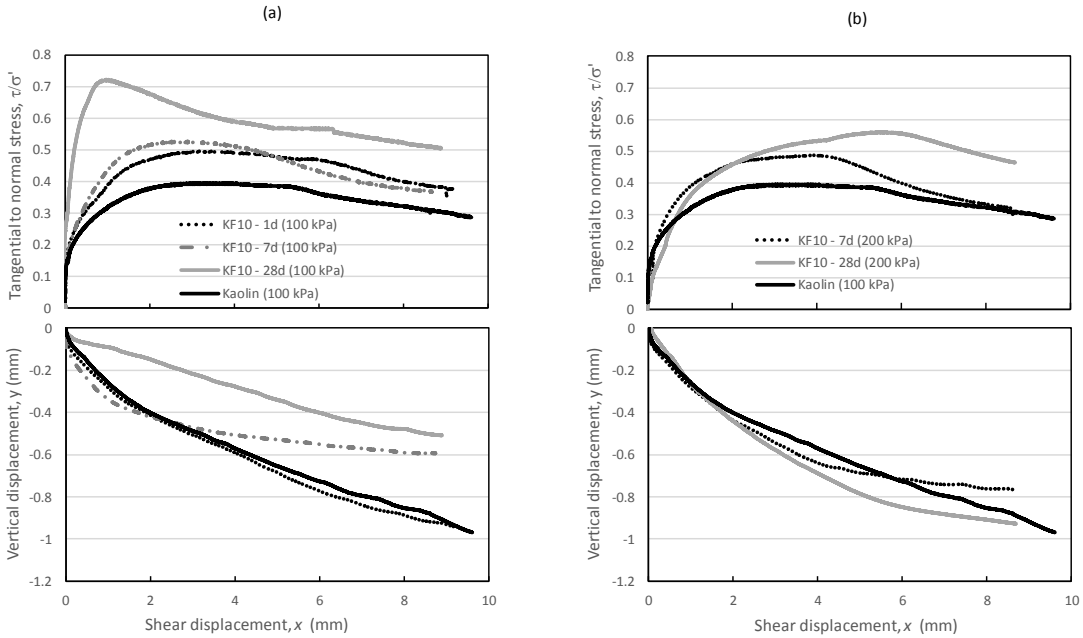

700

701

702 Fig. 4. Direct shear tests on kaolin and alkali activated binder treated kaolin (KF10) at

703 different curing periods. (a) normal stress σ=100 kPa. (b) normal stress σ=200 kPa

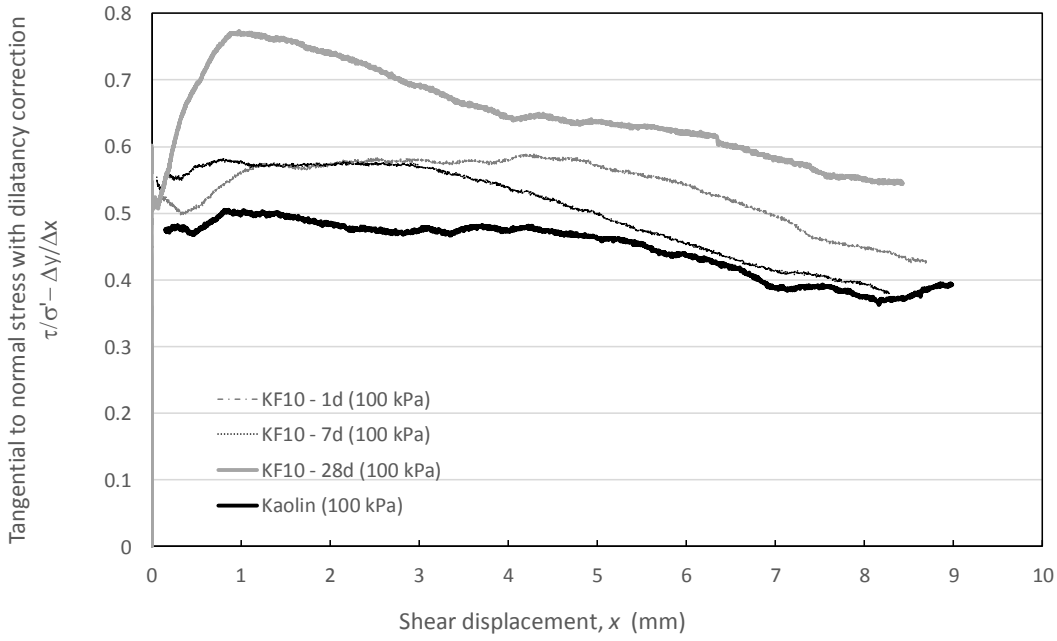

704

705 Fig. 5. Direct shear tests on kaolin and alkali activated binder treated kaolin (KF10) at
706 different curing periods and normal stress σ=100 kPa: shear strength data corrected for
707 dilatancy.

708

709

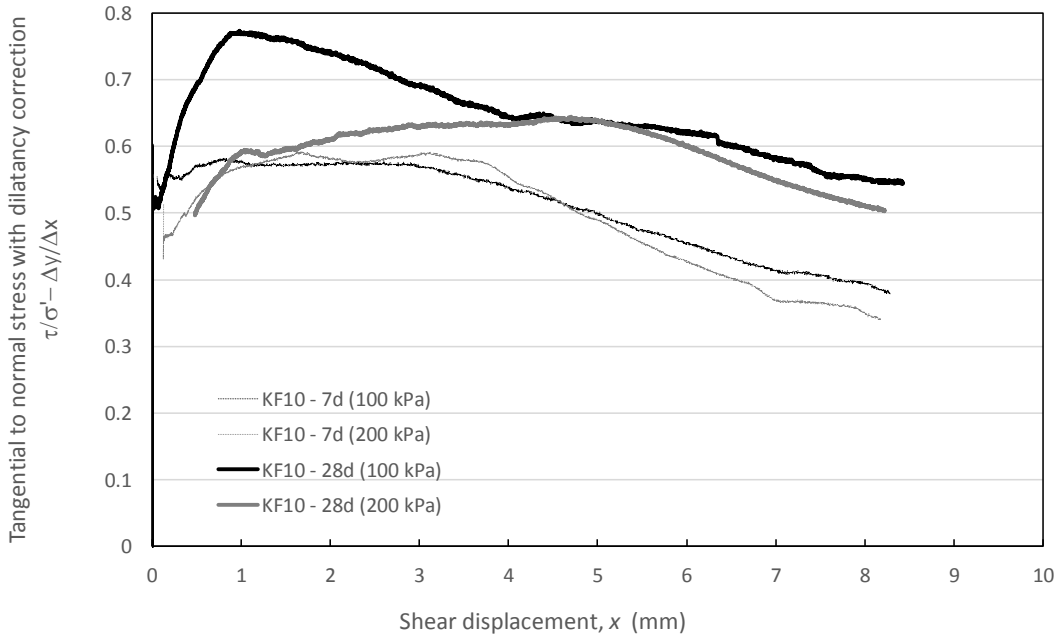

710

711 Fig. 6. Direct shear tests on kaolin and alkali activated binder treated kaolin (KF10) at
712 curing periods 7 and 28 days and normal stresses σ=100 kPa and σ=200 kPa: shear
713 strength data corrected for dilatancy.

714

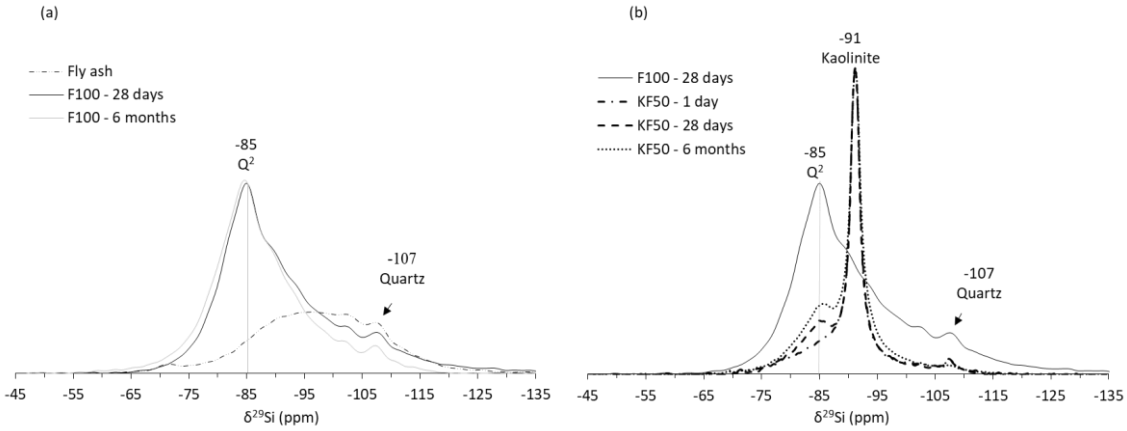

715

716

717 Fig. 7. ^{29}Si MAS-NMR spectra. (a) Raw fly ash and binder F100 at 28 days and 6

718 months. (b) alkali activated binder F100 at 28 days and alkali activated kaolin KF50 at 1

719 and 28 days (after Coudert et al., 2019).

720
721

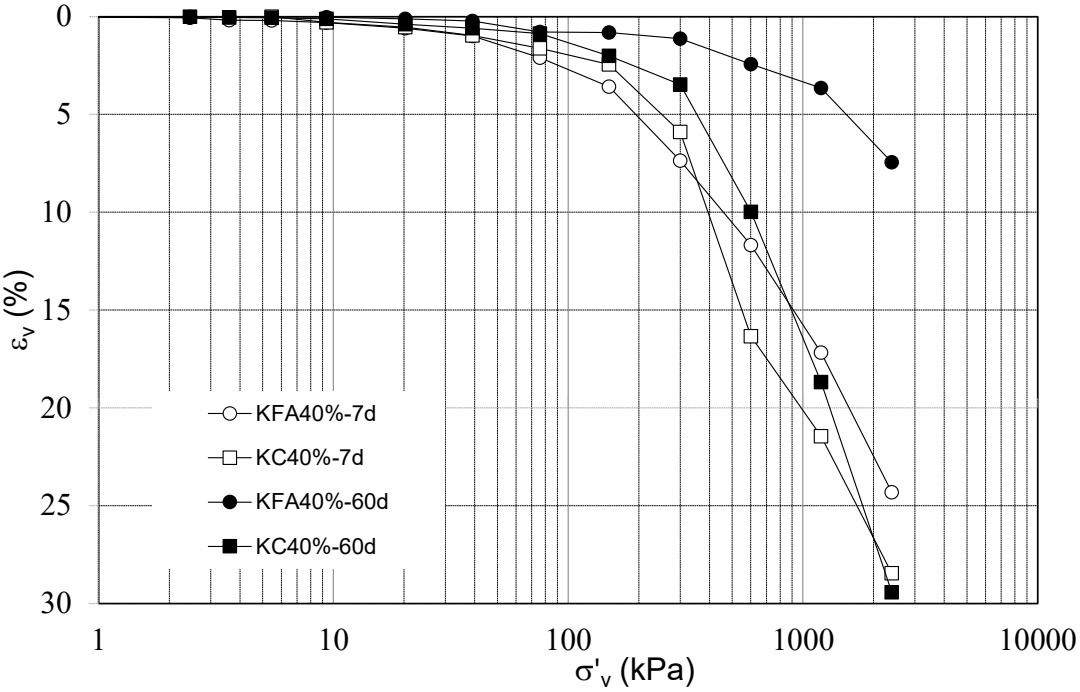

722
723 Fig. 8. Comparison between one dimensional compression tests on alkali activate fly
724 ash binder treated kaolin and ordinary Portland cement treated kaolin cured for 7 and 60
725 days.
726

727

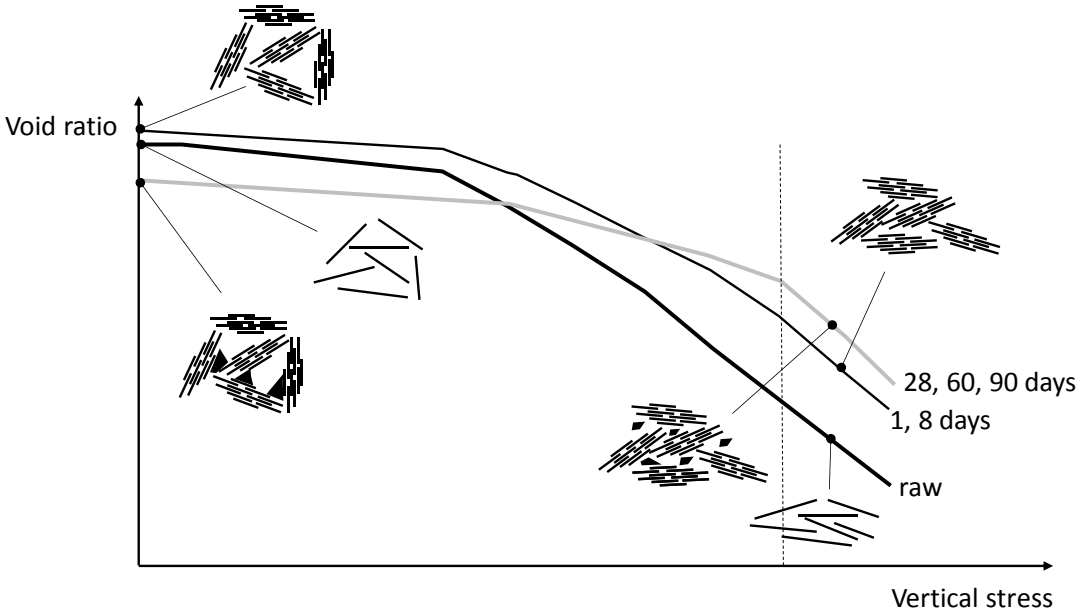

728

729 Fig. 9. Conceptual model for micro-mechanical behaviour of raw kaolin and alkali

730 activated fly ash binder treated clay.

731

732

Mechanical behaviour of compacted kaolin clay stabilised via alkali activated calcium-rich fly ash binder

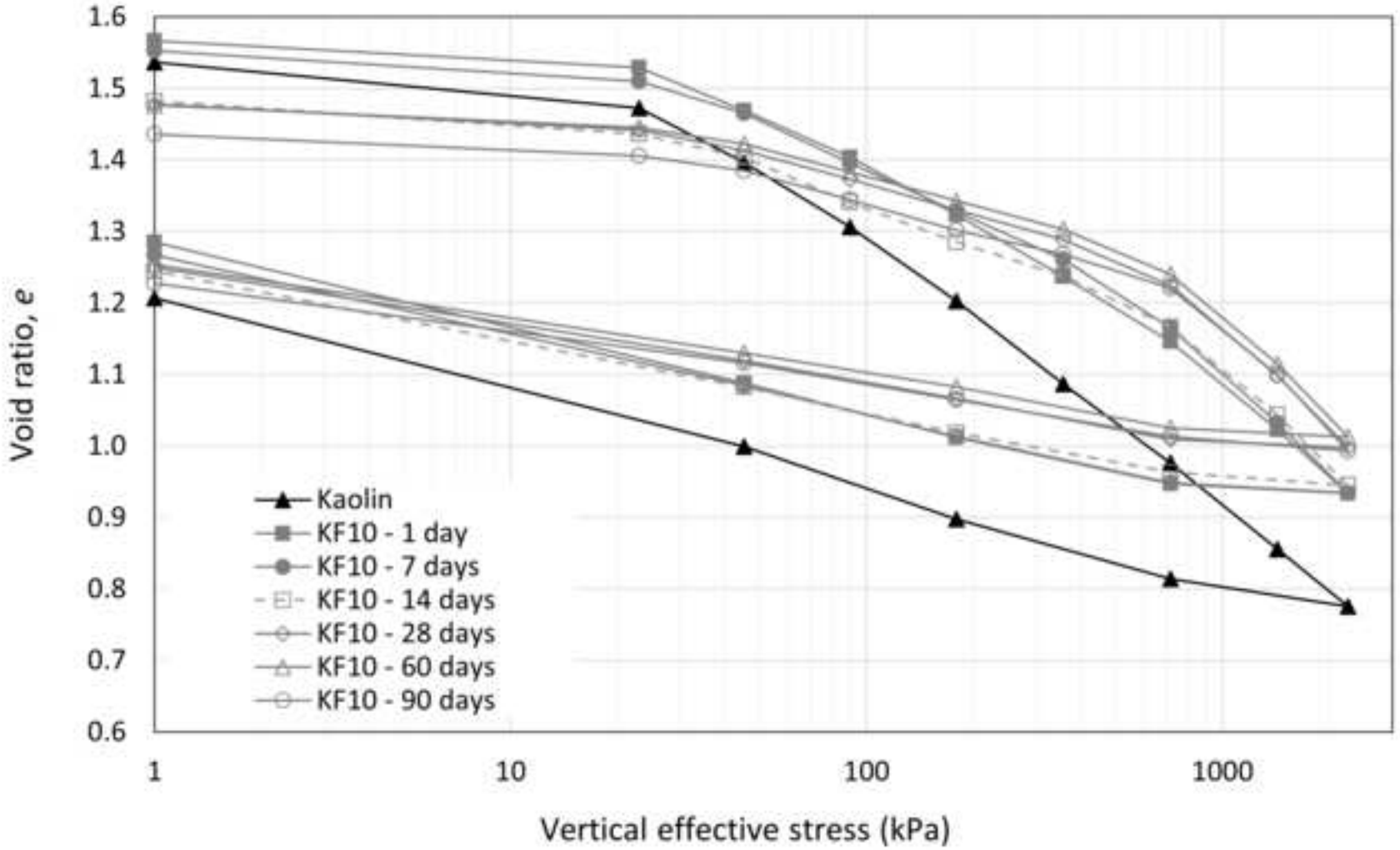

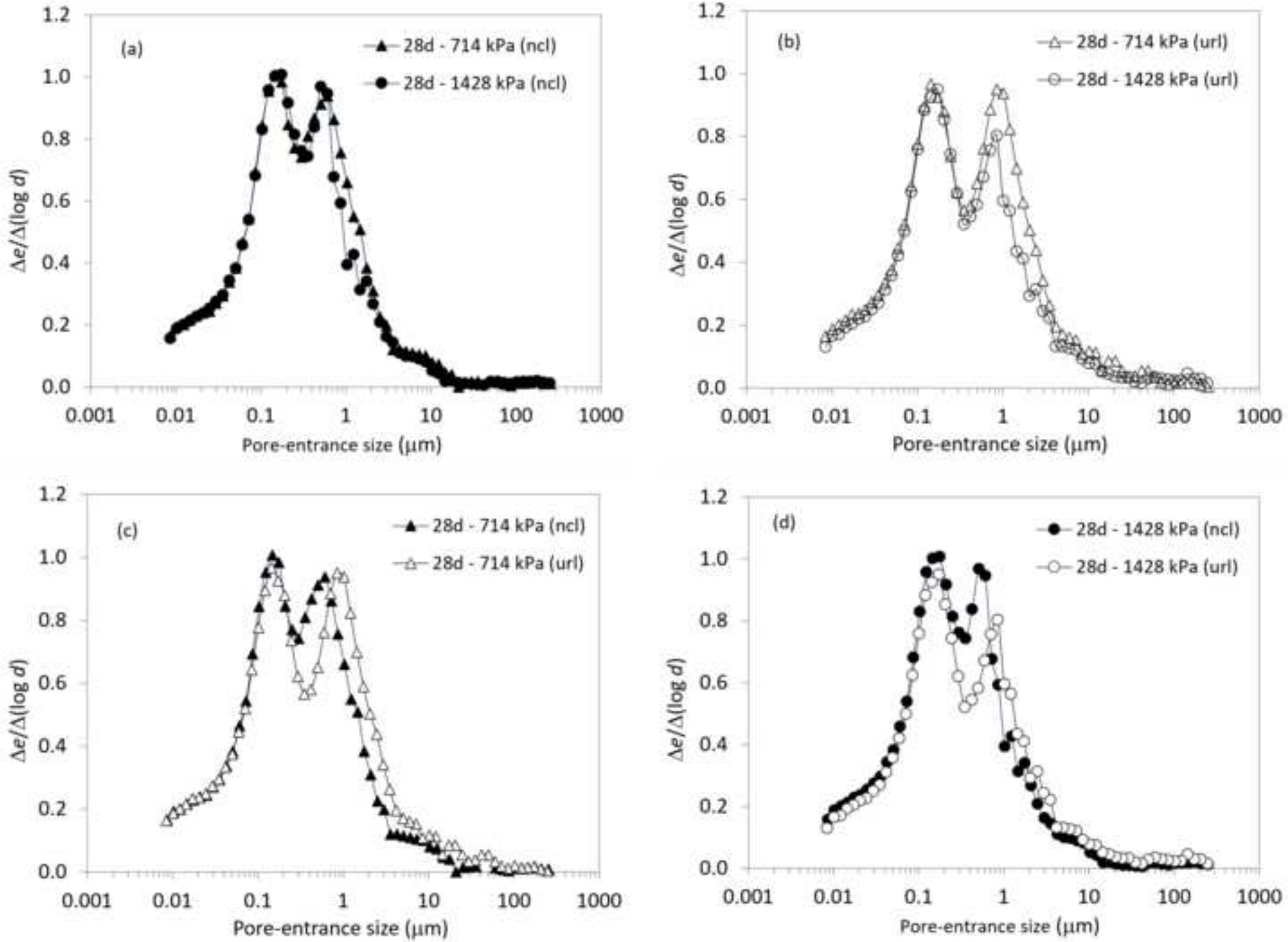

Mechanical behaviour of compacted kaolin clay stabilised via alkali activated calcium-rich fly ash binder

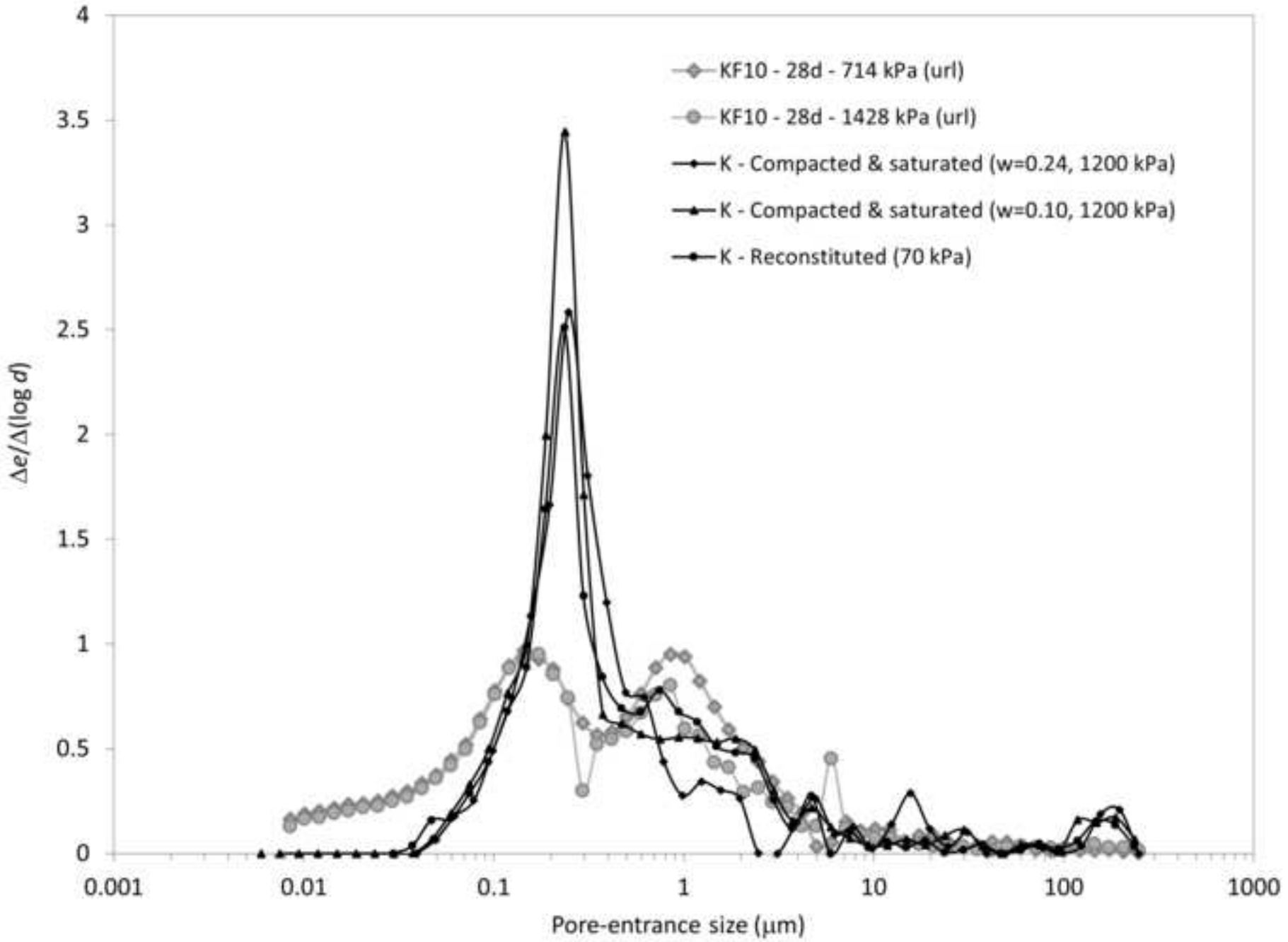

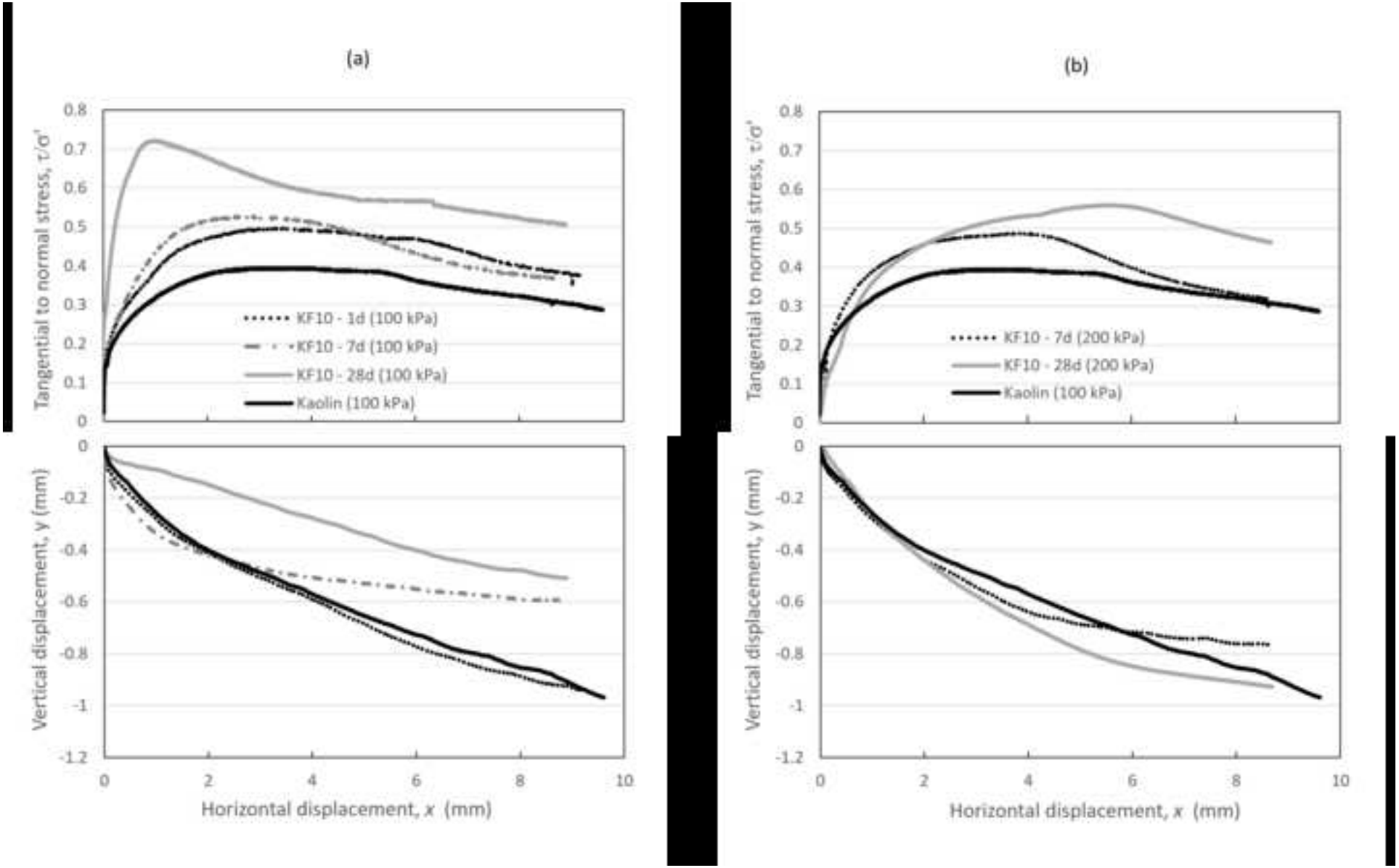

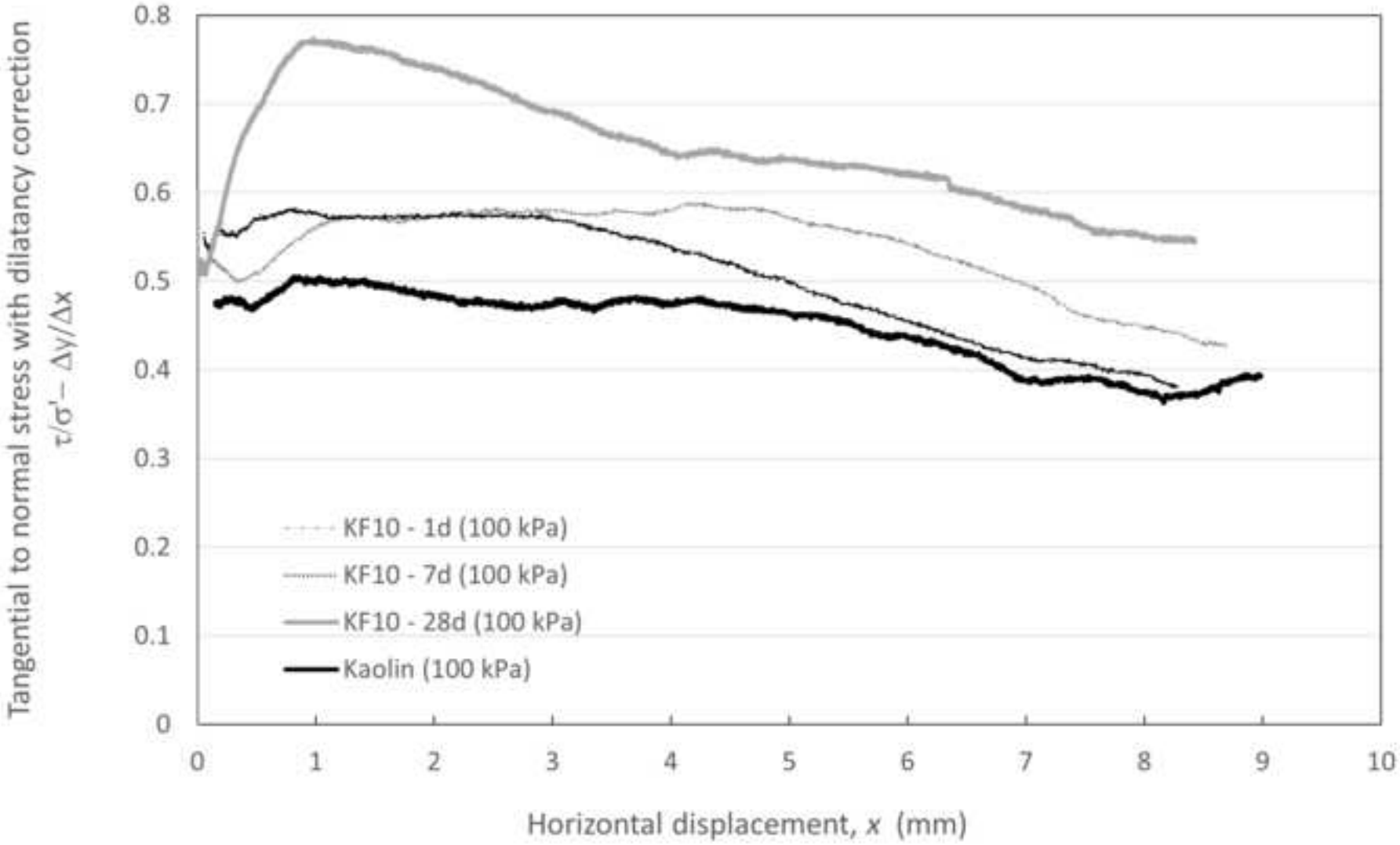

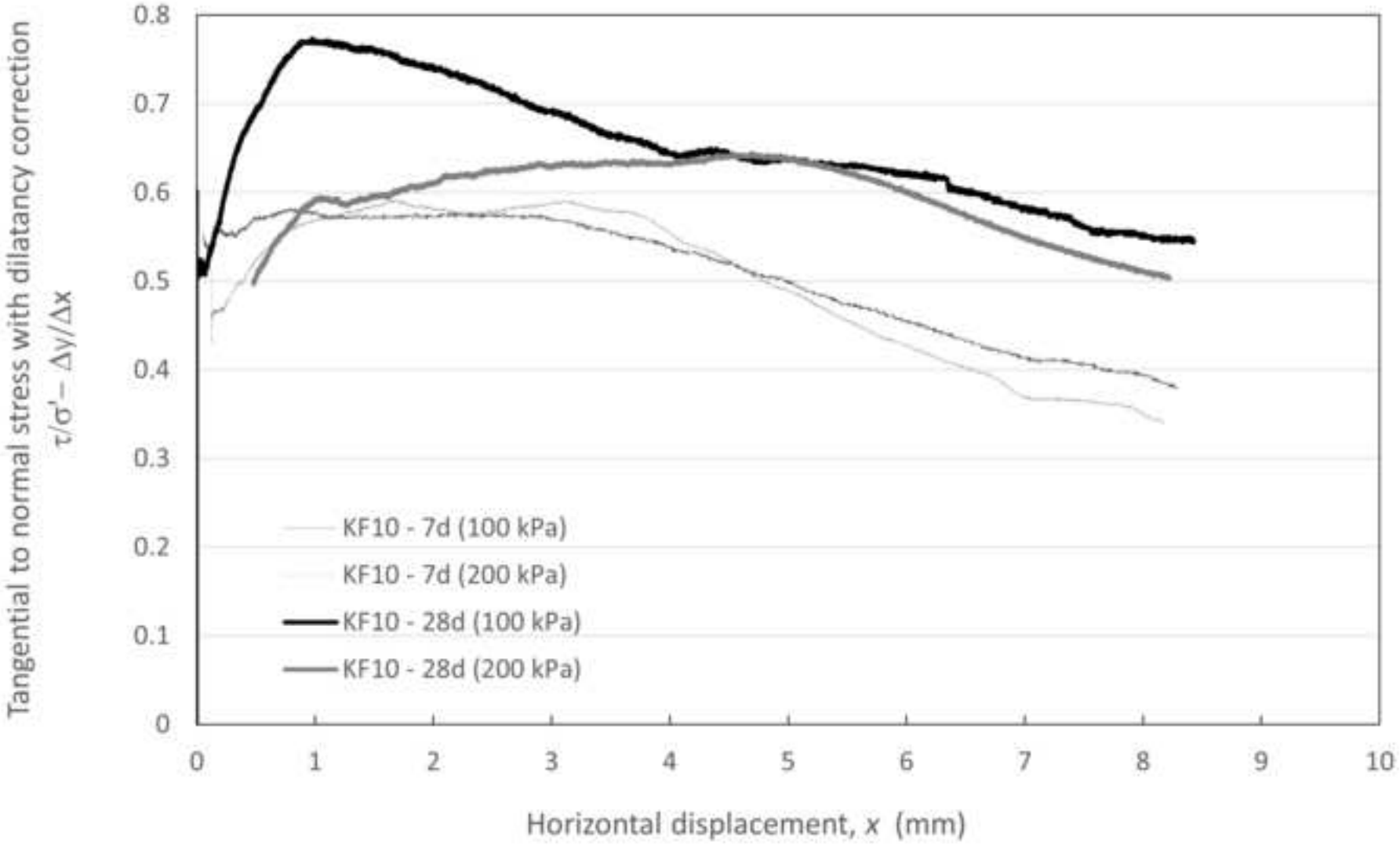

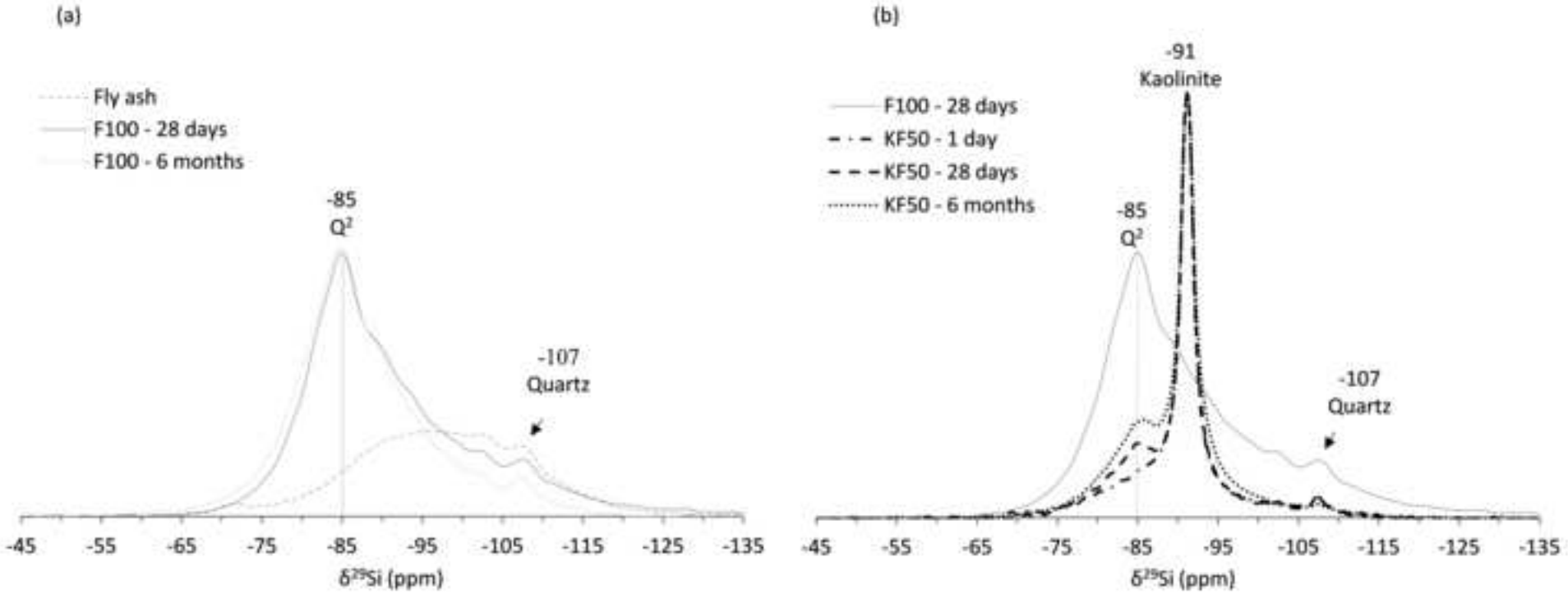

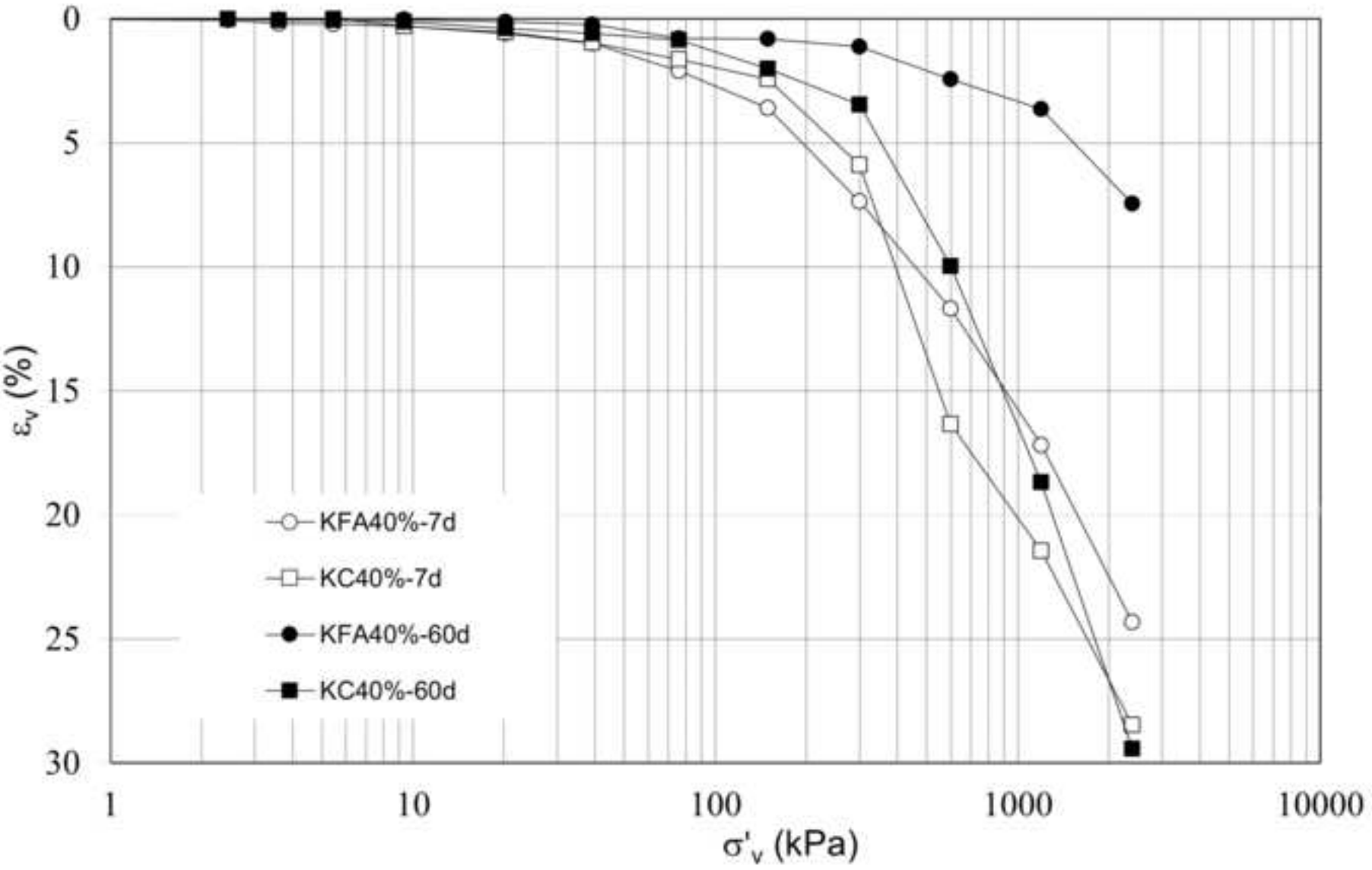

Mechanical behaviour of compacted kaolin clay stabilised via alkali activated calcium-rich fly ash binder

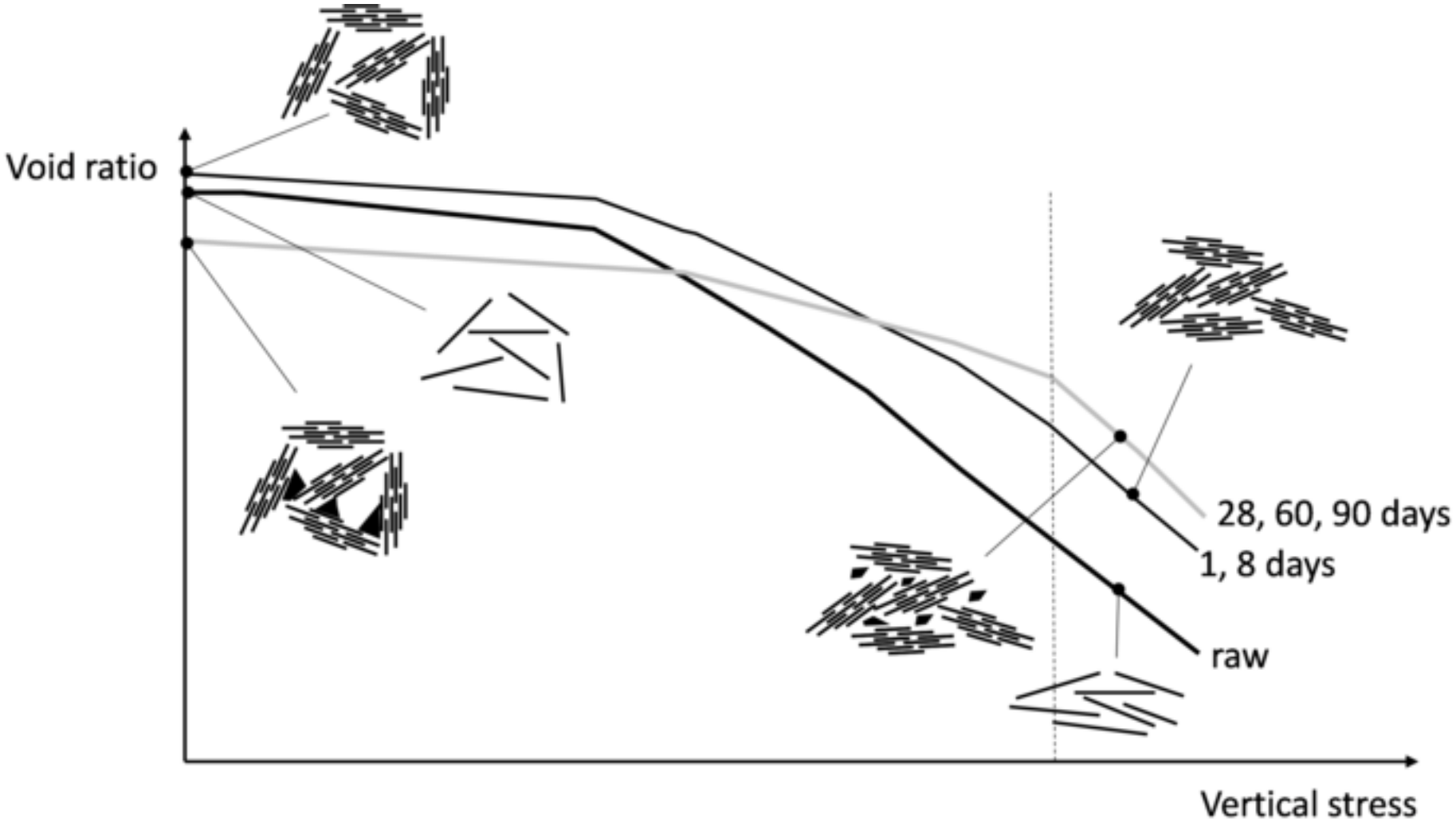

Declaration of interests

☒ The authors declare that they have no known competing financial interests or personal relationships that could have appeared to influence the work reported in this paper.

☐The authors declare the following financial interests/personal relationships which may be considered as potential competing interests:

Credit Author Statement

Author Contributions: Conceptualization and methodology, E.C., D.D., G.R., A.T.; investigation, E.C.; data curation, E.C., G.R., A.T.; writing—original draft preparation, E.C., G.R.; writing—review and editing, A.T., G.R.; supervision, G.R., A.T.

All Authors have read and agreed to the submitted version of the manuscript.